Canugovi *et al. J Cardiovasc Aging* 2022;2:47
DOI: 10.20517/jca.2022.35

The Journal of Cardiovascular Aging

Original Research Article

Open Access

Mitochondrial DAMPs-dependent inflammasome activation during aging induces vascular smooth muscle cell dysfunction and aortic stiffness in low aerobic capacity rats

Chandrika Canugovi[1], Mark D. Stevenson[1], Aleksandr E. Vendrov[1], Andrey Lozhkin[1], Steven L. Britton[2], Lauren G. Koch[3], Marschall S. Runge[1], Nageswara R. Madamanchi[1]

[1]Division of Cardiovascular Medicine, Department of Internal Medicine, University of Michigan, Ann Arbor, MI 48109, USA.
[2]Department of Molecular and Integrative Physiology, Department of Anesthesiology, University of Michigan, Ann Arbor, MI 48109, USA.
[3]Department of Physiology and Pharmacology, The University of Toledo, Toledo, OH 43606, USA.

Correspondence to: Dr. Nageswara R. Madamanchi, Division of Cardiovascular Medicine, University of Michigan, 1150 West Medical Center Drive, 7301A Medical Science Research Building III, Ann Arbor, MI 48109, USA. E-mail: madamanc@med.umich.edu

How to cite this article: Canugovi C, Stevenson MD, Vendrov AE, Lozhkin A, Britton SL, Koch LG, Runge MS, Madamanchi NR. Mitochondrial DAMPs-dependent inflammasome activation during aging induces vascular smooth muscle cell dysfunction and aortic stiffness in low aerobic capacity rats. *J Cardiovasc Aging* 2022;2:47. https://dx.doi.org/10.20517/jca.2022.35

Received: 18 Aug 2022 **First Decision:** 22 Aug 2022 **Revised:** 21 Sep 2022 **Accepted:** 23 Sep 2022 **Published:** 30 Sep 2022

Academic Editors: Junichi Sadoshima, Ali J. Marian **Copy Editor:** Fangling Lan **Production Editor:** Fangling Lan

Abstract

Introduction: Low aerobic exercise capacity is an independent risk factor for cardiovascular disease (CVD) and a predictor of premature death. In combination with aging, low aerobic capacity lowers the threshold for CVD.

Aim: Since low aerobic capacity and aging have been linked to mitochondrial oxidative stress and dysfunction, we investigated whether aged Low-Capacity Runner (LCR) rats (27 months) had vascular dysfunction compared to High-Capacity Runner (HCR) rats.

Methods and Results: A significant decrease in aortic eNOS levels and vasodilation as well as an increase in aortic collagen and stiffness were observed in aged LCR rats compared to age and sex-matched HCR rats. There was a correlation between age-related vascular dysfunction and increased levels of ROS and DNA damage in aortas of LCR rats. Moreover, mitochondrial oxygen consumption, membrane potential, ATP levels, and mitophagy were lower in VSMCs of aged LCR rats. VSMCs from older LCR rats showed AIM2 inflammasome activation. VSMCs of

young (4 months old) LCR rats treated with purified mitochondrial damage-associated molecular patterns (DAMP) recapitulated an inflammasome activation phenotype similar to that seen in aged rat VSMCs. Rapamycin, a potent immunosuppressant, induced mitophagy, stimulated electron transport chain activity, reduced inflammasome activity, mitochondrial ROS and DAMP levels in VSMCs from aged LCR rats. MitoTEMPO, a mitochondrial ROS scavenger, was similarly effective on VSMCs from aged rats.

Conclusion: The findings suggest that impaired mitophagy and inflammasome activation in the vasculature under conditions of low aerobic exercise capacity during aging results in arterial dysfunction and aortic stiffness. In older adults with reduced aerobic capacity, mitochondrial antioxidants, mitophagy induction, and inflammasome inhibition may be effective therapeutic strategies for enhancing vascular health.

Keywords: Oxidative stress, DNA damage, AIM2 inflammasome, mitophagy, mitochondrial bioenergetics, VSMC

INTRODUCTION

Both aerobic exercise capacity and activity are well-established predictors of age-adjusted cardiovascular and overall mortality in both healthy subjects and those with cardiovascular disease (CVD)[1-5]. Peak aerobic exercise capacity declines with age, and the rate of decline increases markedly with each successive decade[6]. A decrease in the peak heart rate, peripheral oxygen consumption, cardiac β-adrenergic receptor density, and postsynaptic β-adrenergic signaling underlies the decline in aerobic capacity associated with aging, which lowers the threshold for CVD development.

Most of the population studies on exercise capacity focus on correlation-based assessment of patients without attempting to infer a causal relationship between the variables. Experimental validation of causal inference, if any, in correlation-based population studies was performed using unique rat models with high and low intrinsic aerobic capacities (High-Capacity Runners, HCR and Low-Capacity Runners, LCR)[7]. Specifically, this was accomplished by genetic segregation via two-way artificial selection based on treadmill exercise tests to investigate the influence of intrinsic aerobic capacity on all-cause mortality and morbidity[8]. The median lifespan for LCR is 28%-45% shorter than that for HCR, and maximal oxygen uptake serves as a reliable predictor of lifespan across adulthood[9]. In addition, for every 10 g gain in body weight during adulthood, lifespan decreased by approximately 1 month in a combined population of male and female rats, indicating that gain in body weight over time is also an important predictor of longevity. Early deaths in LCR may be attributed to pathophysiological mechanisms associated with aging, such as the failure of one or more organs. The LCR rats also exhibit a number of cardiovascular risk factors and impaired mitochondrial oxidative pathways[10].

The impaired mitochondrial oxidative phosphorylation increases mitochondrial reactive oxygen species (ROS) production, resulting in mitochondrial DNA (mtDNA) damage[11,12]. Mitochondrial ROS, in turn, impair mitochondrial respiration, limiting exercise capacity[13,14]. The increased production of mitochondrial ROS, accumulation of mtDNA damage, and progressive respiratory dysfunction contribute to the pathogenesis of CVD[12,15], and a causative link has been established between DNA damage, both nuclear and mitochondrial, and aging-related phenotypes[16-20]. Mitophagy, the selective degradation of mitochondria by autophagy[21], removes the damaged mitochondria to maintain cellular homeostasis[22]. Impairment of mitophagy results in diminished clearance of damaged mitochondria, which releases mtDNA into circulation[23-26]. Known as damage-associated molecular patterns (DAMPs), mitochondria-derived fragments are implicated in the development of chronic (sterile) inflammation in aging[25] via activation of inflammasome[27]. Additionally, mitochondrial dysfunction and chronic systemic inflammation have been linked to obesity[28,29].

The hardening of the central arteries is a hallmark of advancing age, which impacts cardiac function, microcirculation, and organ function[30,31] and is a major cause of age-related CVD[32]. Lower cardiorespiratory fitness is correlated with arterial stiffening in coronary artery disease patients with myocardial infarction[33], and higher cardiorespiratory fitness is correlated with a reduction in age-related arterial stiffness in adults[34]. There is also evidence that obesity accelerates the process of artery stiffening earlier in life[35,36]. It has been proposed that defective mitochondrial quality control contributes to the thickening of large elastic arteries and stiffening with age via mitochondrial stress/dysfunction[30]. However, the molecular mechanisms regulating aortic stiffening are yet to be fully elucidated.

This study examines VSMC function and metabolism in aging at the intersection of low aerobic capacity and obesity phenotype. We hypothesized that reduced aerobic capability in older LCR rats would be associated with impaired vascular function, increased aortic stiffening, elevated mitochondrial oxidative stress, mtDNA damage, impaired mitophagy, and inflammasome activation, along with vascular remodeling.

MATERIALS AND METHODS

Rats: All animal procedures were performed in compliance with the protocols approved by the Institutional Animal Care and Use Committee of the University of Michigan in accordance with NIH OLAW guidelines. The Low-Capacity Runner (LCR) and High-Capacity Runner (HCR) rat models have been described previously[7]. Exercise capacity was the basis for artificial selection in a genetically heterogeneous population of rats (N:NIH outcrossed stock) to isolate LCR and HCR rats. At 11 weeks of age, every rat underwent endurance running tests on a treadmill, and the time and maximal distance it was able to run before exhaustion were monitored. The top 20 percent and the bottom 20 percent of the runners were bred for genetic heterogeneity for 40 generations in order to segregate LCR and HCR rats[9]. We used young (4-month-old, 37th generation) and old (27-month-old, 34th generation) male rats in this study. All rats used in this study were also subjected to a one-time running test at 11 weeks of age to verify whether they had low- or high-running capacities. The data showed that LCR rats were able to run for 11.6 min before exhaustion, while HCR rats were able to run for 75 min before exhaustion, making it a relevant model of aerobic capacity.

RNASeq: RNA was extracted from thoracic aortas of young and old HCR and LCR rats (n = 3) using the Qiagen RNeasy Kit. RNA quality was assessed using an Agilent 2100 Bioanalyzer. All RNA samples had an RNA Integrity Number of ≥ 9.5. Sequencing libraries were prepared at University of Michigan Advanced Genomics Core with TruSeq RNA Library Preparation Kit (Illumina). RNA sequencing was performed on an Illumina HiSeq 4000 platform with three lanes per sample generating 125 bp paired-end reads with an average of 80 million reads per sample. Quality control and alignment for RNA sequencing were performed at the University of Michigan Bioinformatics Core. Raw reads were concatenated into a single FASTQ file for each sample. The quality of the raw reads was checked with FastQC. Reads were aligned to the reference genome (UCSC rn5.fa) using Tuxedo Suite: TopHat and Bowtie2[37]. Cufflinks was used for post-alignment quality control, expression quantification, and normalization. iDEP.91 was used to perform hierarchical clustering, principal component analysis, and differential gene expression analysis with default parameters (Available from: http://bioinformatics.sdstate.edu/idep/)[38]. We identified differentially expressed transcripts and genes using the FDR ≤ 0.05 and fold change ≥ ±1.5. Differentially expressed genes were annotated using gene ontology terms, and pathway enrichment analyses were performed using the g:Profiler g:GOSt web application (Available from: http://biit.cs.ut.ee/gprofiler/gost)[39]. To identify enriched signaling pathways, we used the KEGG Pathway database (Available from: https://www.genome.jp/kegg/pathway.html).

VSMC culture: Four separate VSMC isolates were made from the aortas of young (4-month-old) and old (27-month-old) HCR and LCR rats. Details of the cell isolation protocol were published previously[40]. Briefly, aortic VSMCs were isolated by stripping off the adventitial layer and using only the media for cell isolation. The adventitial and medial layer separation was confirmed by immunostaining with α-SM actin antibody of random samples. Before digestion of the media to obtain VSMCs, calcium alginate swabs were used to remove the endothelium. Aortic rings (< 3 millimeters) were then incubated in collagenase type II and elastase mixture at 37 °C for 1.5 h or until complete digestion with intermittent mixing with a glass Pasteur pipet. Released VSMCs were cultured in DMEM supplemented with 10% FBS, antibiotics, and Amphotericin B (Gibco). Experiments were performed with cells from passages 3-10. Gene expression analysis of *Acta2* (Actin Alpha 2, Smooth Muscle), *Myh11* (Myosin heavy chain 11), and *Cnn2* (Calponin 2) confirmed the phenotype of VSMCs in all isolates.

ROS detection: Incubation of frozen aortic sections or cultured VSMCs in Hank's balanced salt solution containing 1 mM $CaCl_2$ and 1 mM $MgSO_4$ for 15 min was performed in the presence of 10 μM dihydroethidium (DHE) (Invitrogen) or 5 μM MitoSOX Red and 200 nM MitoTracker Green FM (where indicated). A Nikon Eclipse Ti was used to image MitoSOX or DHE fluorescence (read between 565 nm excitation and 635 nm emission) at equal exposure, gain, and offset. NIH Image J software was used to evaluate fluorescence intensity by counting average gray values per area within a defined region of interest (ROI).

Immunofluorescence: For Immunofluorescent staining, the tissues or cells were fixed in 3.6% formaldehyde for 20 min at room temperature and permeabilized in 0.05% Triton X-100 for 3 min, followed by 3 × 5 min washings in PBS. The fixed tissues or cells were incubated with primary antibodies [Supplementary Table 1] overnight at 4 °C according to the manufacturer's instructions. Thereafter, the tissue was washed three times with PBS and incubated with an Alexa Fluor-conjugated secondary antibody for 2 h. The Auto-fluorescence was quenched with TrueVIEW kit (Vector laboratories). The slides were mounted in mounting media containing DAPI (H100, Vector labs).

Picrosirius red staining: The aortic sections were fixed in acetone and cold methanol for 30 min each. Sections were stained with Picrosirius red kit (Abcam). The excess stain was washed off twice with acetic acid, and the slides were dehydrated with ethanol. Sections were mounted using Vectashield H100 mounting medium without DAPI. The images were acquired under brightfield using a Nikon TI-E camera attached to an upright E600 microscope at equal exposure time for all images. NIH Image J was used to measure the area of picrosirius red staining in the aortic media.

Lipofuscin staining: The VSMCs were cultured in 8-well chambered glass slides until 80% confluency was reached. Cells were washed twice with PBS at room temperature, then incubated for 3 min in cold Glutaraldehyde fixative solution (25 mL acetone and 75 mL glutaraldehyde solution) for 3 min and washed thoroughly with PBS. Next, cells were stained with Sudan Black B staining reagent (Sigma Aldrich) for 5 min. The excess stain was removed by washing three times with 70% ethanol, followed by deionized water. The slides were mounted in VectaMount AQ (Vector Laboratories Inc.). Images were acquired using a Nikon TI-E camera attached to an upright E600 microscope under brightfield at equal exposure times. Perinuclear and cytoplasmic dark blue/black staining was measured using NIH Image J as an integrated density (mean gray value per area).

Mitophagy: VSMCs were cultured in 8-well chambered slides until 60% confluency was reached. Cells were incubated for 30 min at 37 °C with Mtphagy dye (Mitophagy kit, Dojindo), followed by mitophagy-inducing

compounds or vehicle for 16 h. The cells were washed twice with PBS and then exposed to Lyso dye (Mitophagy kit, Dojindo) for another 30 min at 37 °C, according to the manufacturer's protocol. The slides were washed twice with 1xPBS and mounted in mounting media containing DAPI (H100, Vector labs). All slides were imaged by Nikon Eclipse Ti- fusion microscope with DAPI, FITC and Texas Red Channels at equal exposure, gain and offset. The colocalization of mtphagy and lyso dyes (yellow color) was quantified by NIH Image J as integrated density per area of interest. An indicator of mitophagy flux is the ratio of colocalization signals in induced samples to those in uninduced samples. We then measured autophagic vacuole formation using the CYTO-ID kit (ENZ-KIT175-0050, ENZO) according to the manufacturer's protocol. Briefly, the VSMCs were cultured until 80% confluency in 8-well chambered slides. The attached cells were incubated with the working solution containing CYTO-ID dye for 30 min at 37 °C. This was followed by two washes with 1xPBS and mounting in mounting media containing DAPI (H100, Vector labs) and imaging.

Flow cytometry: The cells were detached by trypsinization, then placed in a 70 μM cell strainer (Corning, Corning, NY) and washed with FACS buffer (PBS, 1% BSA, 1 mM EDTA). The cells were stained with Apoptosis, DNA Damage and Cell Proliferation Kit (562253 BD Biosciences, Franklin Lakes, NJ) following the manufacturer's instructions. The cells were processed using the ZE5 cellular analyzer (Bio-Rad, Hercules, CA) and the data were analyzed with FlowJo v10 (FlowJo, LLC, Stanford University, CA).

Measurement of ATP levels: Cellular ATP levels in both young and old HCR and LCR VSMCs were measured using a bioluminescence ATP determination kit (ThermoFisher), following the manufacturer's instructions. In this assay, ATP reacts with luciferin in the presence of luciferase, converting it into oxyluciferin. As a result, the light produced is proportional to the cellular ATP levels[41]. In brief, equal volumes of VSMC protein lysates were incubated with a reaction buffer containing D-luciferin (500 M), firefly luciferase (1.25 g/mL), and 1 mM (DTT). The luminescence was measured with a luminometer, and ATP levels were determined using a standard curve generated simultaneously.

Western blotting: VSMC and aortic protein lysates were prepared using M-PER and T-PER lysis buffers, respectively, and the protein concentration was determined using BCA assay (ThermoFisher). Equal amounts of proteins were loaded on SDS-PAGE gels and were separated by electrophoresis. The proteins were then transferred onto nitrocellulose membranes using a semi-dry Western transfer apparatus (Trans-Blot Turbo system, BioRad). The blots were blocked with Blocker™ BSA (ThermoFisher) and probed overnight with primary antibodies (AIM2, Caspase1, VCAM, LAMP1 from Santa Cruz; IL18, TOM20 from Abcam; FITC- tagged-ACTA2 from BIOS). Blots were washed 3 × 5 min with PBST (PBS + 0.1% TWEEN 20), then stained with IRDye 800CW (green) or IRDye 680RD (red) secondary antibodies (LI-COR) for 1 h at room temperature. The blots were imaged with a near-infrared fluorescence digital detection scanner, Odyssey CLx (LI-COR).

Mitochondrial bioenergetics: The mitochondrial bioenergetics of rat VSMCs were measured using the Seahorse XFp and XF96 machines (Agilent technologies). Approximately 20,000 cells were cultured in DMEM supplemented with 10% FBS and antibiotics in cell culture microplates supplied with Flexpack (Agilent technologies) for 24 h. The next day, the media were changed to phenol-red free basal DMEM (Agilent technologies) supplemented with 25 mM glucose, 2 mM pyruvate, and 1 mM glutamine, and incubated in a CO_2-free incubator at 37 °C for least 1 h before analysis. Cellular oxygen consumption rate (OCR) at basal level and in the presence of 2 M oligomycin, 500 nM trifluoromethoxy carbonylcyanide phenylhydrazone (FCCP) and 500 nM rotenone + antimycin A was quantified in three consecutive cycles for 3 min each. Pre-treatment of cells with 20 nM rapamycin or 10 nM MitoTEMPO were performed where

indicated for 16-18 h. In order to normalize the OCR values to protein levels, the cells were lysed with M-PER buffer and the protein content was determined by BCA assay.

Mitochondrial DNA damage analysis: The total genomic DNA of rat aortas was isolated with a Qiagen blood and tissue kit. The DNA concentration was determined using two different methods, the Nano-Drop ND-1000 spectrophotometer and the Quant-iT PicoGreen dsDNA Assay Kit (Thermo Fisher Scientific). Equal amounts of DNA were used as a template to amplify a 13.4 kb mitochondrial DNA fragment. We used rat-specific primers (Forward: AAA ATC CCC GCA AAC AAT GAC CAC CC, Reverse: GGC AAT TAA GAG TGG GAT GGA GCC AA)[42] and Takara LA Taq™ long DNA polymerase (Takara Bio USA) for amplification of mitochondrial DNA in a polymerase chain reaction. An equal aliquot of the PCR product was run on an agarose gel to determine the quality and densitometry to determine the quantity of the expected size band. The amount of amplification product from the long-fragment PCR was normalized by measuring the levels of MTCO1 in the DNA template in a separate quantitative PCR reaction using a Taqman probe.

Cell-free DNA isolation and amplification: An equal number of VSMCs from young and old LCR and HCR rats were plated in 6-well culture dishes. After 30 h of incubation, the media were spun down at 2000 xg for 5 min to remove floating cells and debris. The DNA was extracted in 500 µL of cell-free medium from each sample using a blood and tissue kit (Qiagen). The exuded DNA was measured using a Nano-Drop ND-1000 spectrophotometer, and equal volumes of DNA were used as templates in a quantitative PCR (ABI 7500 Real-time PCR machine). A fragment spanning 80 base pairs from the MTCO1 gene was amplified using the Taqman probe (Applied Biosystems). The experiment was repeated at least three times, and the average cycle number (Ct) was plotted. The Ct value is inversely proportional to the amount of circulating mtDNA. For *in vivo* circulating mtDNA analysis, we used 300 µL of plasma from at least three different rats.

DAMPs preparation: MtDNA was isolated from rat liver mitochondria using DNA blood and tissue kit (Qiagen). Firstly, mitochondria were isolated with mitochondrial isolation kit (Pierce), and then mitochondrial pellets were used to isolate DNA. DNA was sonicated up to 5 cycles on ice, at a low setting, each for 30 s, spaced by 1-min intervals. The DNA samples before and after the sonication were run on 1.5% agarose gel to determine the size of the fragmented DNA samples. A length of 150 to 250 base pairs was considered optimal to induce inflammasome activation in cells.

Wire myography: The vascular function analysis was performed using a Danish Myo Technology wire myograph (DMT 620 MS, ADInstruments, Inc., Colorado Springs, CO) as described[16]. In brief, the mesenteric arteries were freshly isolated and immediately mounted using 25 µm tungsten wires to the jaws of the DMT myograph. The vessels were kept in physiological saline solution (PSS; 130 mM NaCl, 4.7 mM KCl, 1.18 mM KH_2PO_4, 1.17 mM $MgSO_4 \cdot 7H_2O$, 14.9 mM $NaHCO_3$, 5.5 mM dextrose, 0.026 mM $CaNa_2$-EDTA, 1.6 mM $CaCl_2$, pH~7.4) throughout the test. The vascular reactivity to contraction with phenylephrine (PE, 10^{-9}-10^{-5} M) and endothelium-dependent relaxation with acetylcholine (ACH, 10^{-8}-10^{-5} M) was determined by stepwise half-log dose increases. Data were recorded using PowerLab software (LabChart, ADInstruments, Inc.).

Pressure myography: The descending thoracic aorta segments were isolated from LCR and HCR rats (n = 7). The tissues were mounted with 6-0 nylon sutures so that aortic segments (approximately two to three millimeters in length) between intercostal arteries could be pressurized in a large vessel chamber of a pressure myograph system (Living Systems Instrumentation, Burlington, VT). Aortic segments were

incubated in Ca^{2+}-free PSS (130 mM NaCl, 4.7 mM KCl, 1.18 mM KH_2PO_4, 1.17 mM $MgSO_4 \cdot 7H_2O$, 14.9 mM $NaHCO_3$, 5.5 mM dextrose, 0.026 mM EDTA, 1.6 mM EGTA, pH~7.4) for 20 min at 37 °C before testing. Initially, vessel had an internal pressure of 10 mmHg, and pressure was increased by 20 mmHg incrementally while allowing time for the vessel to stabilize (< 1 min). The external diameter of each vessel (opacity prevented visualization of internal diameters) was recorded at each increment up to 190 mmHg pressure using a video dimension analyzer calibrated to a 2X objective with a 0.35X c-mount lens (Nikon). Strain (ε) of the vessel was calculated using the formula $\varepsilon = (D_i - D_o)/D_o$, where D_i represents the external diameter at a given pressure and D_o represents the initial lumen diameter at 10 mmHg pressure. Pressure vs strain data was fitted to a simple exponential formula $P = \alpha * e^{(\beta\varepsilon)}$, where α is a constant, and β represents a measure of relative vascular stiffness[43,44].

Statistics: All biochemical experiments were repeated at least three times. All analyses were performed with Prism 8 (GraphPad Software). All data were examined for normality using the Shapiro-Wilk test. Where applicable, data were analyzed using an unpaired 2-tailed *t*-test. For experiments involving more than two groups, one-way ANOVA with Tukey post-hoc tests were used. Differences were considered significant at $P < 0.05$.

RESULTS

The interplay between aerobic exercise capacity and aging affects arterial function, inducing aortic stiffening

The development of aortic stiffening is a key feature of aging and an independent predictor of cardiovascular events in hypertensive patients as well as in the general population[45-47]. In this study, we investigated the interaction between exercise capacity, aging, and arterial stiffness. First, we investigated the vasomotor function of mesenteric artery rings by wire myography; however, it did not indicate any significant differences in phenylephrine-induced maximum contraction between old age LCR and HCR rats [Figure 1A]. We then measured acetylcholine (ACH)-induced relaxation of mesenteric arteries from young and old age rats. The relaxation response to ACH was similar in young LCR and HCR rats [Figure 1B]. However, relaxation of the mesenteric arteries from old age LCR rats was significantly smaller than that from old age HCR rats at lower concentrations of ACH, with a marked rightward shift in the concentration-response curve [Figure 1C] and a smaller half-maximal relaxation response [-log(EC50); Figure 1D].

We asked whether a decrease in eNOS expression might be responsible for arterial dysfunction in old LCR rats, since nitric oxide derived from eNOS is important for vascular function. The Western blot analysis of aortic lysates of old age LCR rats revealed a 40% reduction in eNOS protein expression in comparison with the old HCR rats [Figure 1E]. In order to find out if attenuated eNOS phosphorylation and inhibition of its activity contribute to arterial stiffening with low aerobic capacity and aging[48], we analyzed the expression of phospho-eNOS (Ser1177) in the aortas of old LCR and HCR rats. The phospho-eNOS levels in old HCR rats were higher than in old LCR rats [Figure 1F], suggesting that endothelial dysfunction in mesenteric arteries and aortas of LCR rats with aging may be due to reduced eNOS protein expression and activity.

To determine the effects of low aerobic capacity on the function of large conduit arteries during aging, we measured the aortic stiffness of thoracic aortic segments using pressure myography. There was no difference in aortic plasticity between young LCR and HCR rats [Figure 1G]. In contrast, the old LCR rats showed a significant increase in aortic stiffness compared to age-matched HCR rats [Figure 1H and I, $P = 0.0002$]. The remodeling of the extracellular matrix is a major contributor to vessel wall stiffness in aging, and collagen deposition and cross-linking are key to this process[16,49,50]. We stained fresh frozen aortic cross sections with picrosirius red to measure the collagen content. Aortic collagen levels were not different in young LCR and

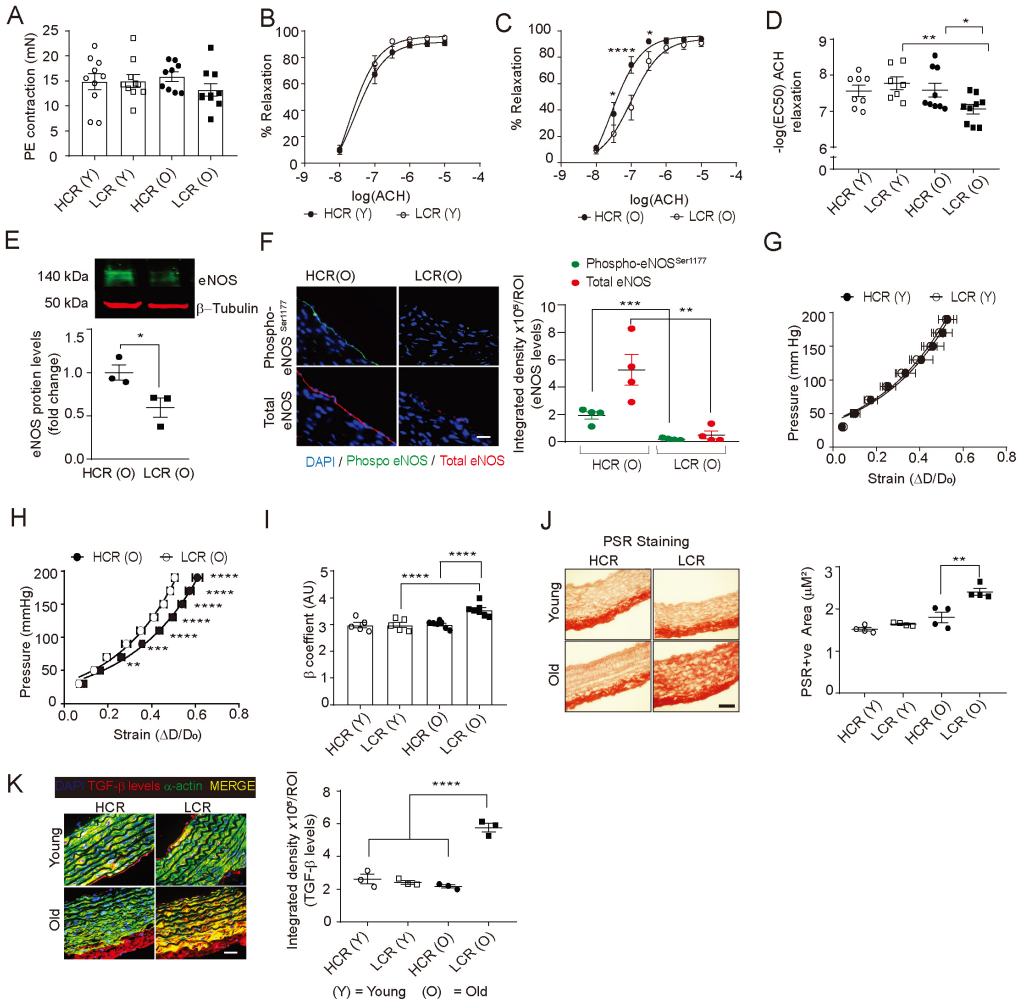

Figure 1. Increased vascular dysfunction, fibrosis, and stiffness in LCR rats with aging. The contractile force in mesenteric artery rings of young (4-month old) and aged (27-month old) LCR and HCR rats in response to phenylephrine (PE) was measured by wire myography (mean ± SEM; *n* = 5) (A). Concentration-response curves for acetylcholine (ACH) induced relaxation of mesenteric arteries from young (B) and old age (C) LCR and HCR rats (mean ± SEM; *n* = 5). Half-maximum relaxation concentration of ACH [-log(EC50)] was calculated from independent dose-response curves and plotted as mean ± SEM, *n* = 5 (D). Representative Western blot of eNOS protein expression in aortic lysates. Densitometry analysis of eNOS protein levels normalized to *β*-tubulin levels (mean ± SEM, *n* = 3) (E). Representative fluorescence images of aortic cross sections stained for immunoreactive total eNOS (red) or phospho-eNOS Ser1177 (green). Data are presented as mean integrated density/ROI ± SEM where *n* = 4 [(F), scale = 50 μm)]. Pressure vs strain data of thoracic aorta segments from young (G) and old (H) LCR and HCR rats were analyzed using pressure myography. The relative stiffness coefficient (H) was calculated by fitting pressure vs strain data to an exponential formula (mean ± SEM, *n* = 5) (I). Representative images of rat aortic cross sections stained with Picrosirius red (PSR) (J). Representative fluorescence images of aortic cross sections co-stained for TGF-*β* (red) and SM-α-actin (green). Bright yellow fluorescence indicates colocalization of TGF-*β* and SM-α-actin. Data are presented as mean integrated density/ROI ± SEM where *n* = 4 (K). *$P < 0.05$; **$P < 0.01$; ****$P < 0.0001$.

HCR rats [Figure 1J]. Conversely, old LCR aortas have a 34% higher collagen content than old HCR aortas [Figure 1J, $P < 0.01$]. Because eNOS-deficient mice have elevated TGF-1β and collagen I levels in their aortas[51], we investigated whether a decrease in eNOS expression or activity in old LCR rat aortas was associated with increased TGF-1*β* expression. Interestingly, TGF-1*β* levels were 2.7-fold higher in old LCR rat aortas than in old HCR aortas [Figure 1K]. An increase in TGF-1*β* expression causes VSMCs to undergo phenotypic changes, upregulating contractile proteins, collagen synthesis and secretion, and enhancement of intrinsic cellular and ECM stiffness, decreasing aortic compliance[52]. The data suggest that low aerobic

capacity in old age impairs endothelial NOS and alters the VSMC phenotype, causing dysregulation of vascular wall homeostasis and aortic stiffening.

Aging is characterized by increased inflammation and necroptosis pathways in the aortic transcriptome of LCR rats

In order to examine how aging and low aerobic capacity impact vascular phenotype at the global level, we performed genome-wide RNA sequencing analysis and compared the transcriptional profiles and signaling pathways enriched in the aortas of young and old HCR and LCR rats. In a hierarchical cluster analysis of the top 1000 most variable genes, there was a distinct separation between young and aged rats, as well as between HCR and LCR rat aortas [Figure 2A]. A principal component analysis showed that old LCR aortas have different transcription profiles from old HCR aortas, besides the obvious differences between young and old rat aortas [Figure 2B]. In the comparison of significantly differentially expressed genes (FDR ≥ 0.05 and fold change ± 1.5) among all groups, the largest differences were found between old HCR and old LCR aortas [Figure 2C]. Transcription analysis revealed a unique expression pattern between old LCR and old HCR aortas with over 1100 genes differentially expressed [Figure 2D].

Compared to old LCR aortas, HCR aortas had 555 upregulated genes and 560 downregulated genes. By contrast, the differentially expressed genes in young HCR aortas were 168 upregulated and 160 downregulated compared with those in young LCR aortas. A gene ontology pathway enrichment analysis focused on selected signaling pathways defined in the KEGG database was conducted to better understand phenotypic changes defined by transcriptional profiles. Significantly differentially upregulated transcripts in old HCR aortas were related to longevity regulating pathways, growth factor signaling pathways (insulin, AMPK, glucagon, and neurotrophin signaling), oxidative phosphorylation, DNA/RNA sensing (RIG-I receptor signaling), and mitophagy/autophagy pathways[Figure 2E]. In contrast, genes significantly upregulated in old LCR aortas were associated with cell cycle regulation (p53 and FoxO signaling) and pro-inflammatory pathways (AGE-RAGE, TGF-β, Toll-like receptor, NF-kappa B, and chemokine signaling) and apoptosis/necroptosis/ferroptosis regulating pathways [Figure 2F]. Based on pathway enrichment analysis, old LCR aortas have reduced mitochondrial biogenesis and mitophagy, increased damage and cytosolic accumulation of DNA/RNA, pro-inflammatory pathway activation, and enhanced apoptosis and necroptosis.

Low aerobic capacity in old age is associated with increased mitochondrial oxidative stress, mitochondrial DNA (mtDNA) damage and dysfunction

We and others have demonstrated that mitochondria-derived oxidative stress increases with aging and affects vascular function and arterial stiffness in animal models and humans[16,40,53-55]. VSMC plasticity plays a pivotal role in vascular remodeling in aging[56,57], which is why we investigated many mechanisms of mitochondrial dysfunction in both the aorta and VSMCs to determine how low aerobic exercise capacity impacts VSMC function. VSMCs isolated from 4-month-old rats did not show any differences in proliferation or senescence between LCRs and HCRs. Aortic ROS levels and mitochondrial ROS levels (mtROS) were measured in aortas as well as in the aortic VSMCs of young and old LCR and HCR rats. Aortic ROS levels measured by DHE fluorescence were not significantly different between both young and old age LCR and HCR rats [Supplementary Figure 1]. However, a higher percentage of VSMCs from old LCR rats had comet tails than VSMCs from old HCR rats, indicating increased nuclear DNA damage [Supplementary Figure 2A]. This was supported by increased nuclear 8-OHdG levels in VSMCs from old LCR rats [Supplementary Figure 2B]. Increased nuclear DNA damage in VSMCs from old LCR rats was accompanied by decreased levels of nuclear γ-H2AX [Supplementary Figure 2C]. An RNA-Seq analysis showed significantly lower superoxide dismutase 2 expression levels in VSMCs from old LCR rats compared to old HCR rats (P = 0.0378). The MitoSOX Red fluorescence measurements of the aortic

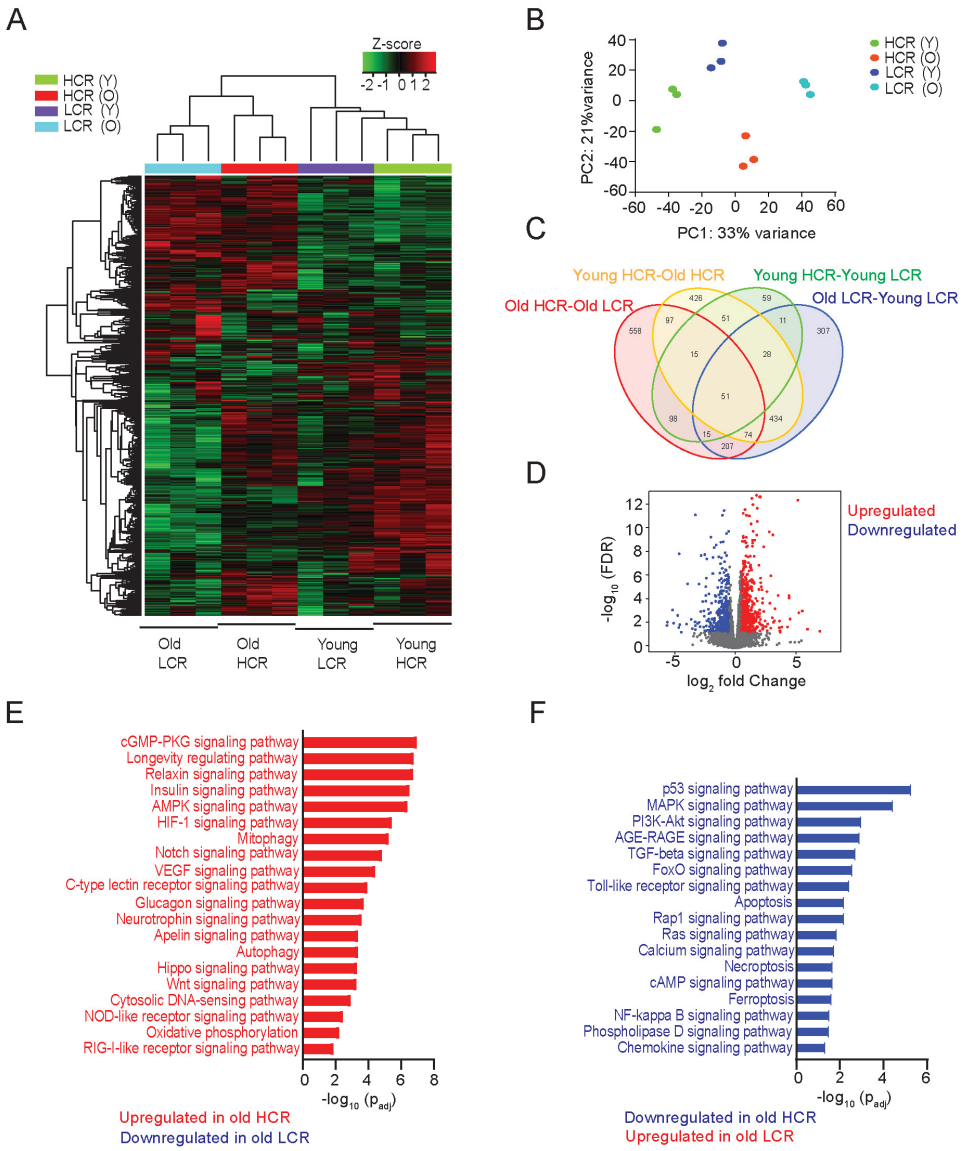

Figure 2. Genome-wide RNA sequencing analysis of aortas from young and old HCR and LCR rats. (A) Heat map representation of unsupervised hierarchical clustering analysis with top 1000 most variable genes. (B) Principal component analysis of the whole transcriptome from young and old HCR and LCR aortas. (C) Venn diagram of differentially expressed genes across four comparisons between young and old HCR and LCR aortas. (D) Volcano plot of differentially expressed genes between old HCR and LCR with FDR ≥ 0.05 and fold change ±1.5. Gene ontology pathway enrichment analysis showing top selected KEGG signaling pathways upregulated (E) or downregulated (F) in old HCR compared with old LCR aortas.

mitochondria of young LCR and HCR rats did not reveal any differences [Figure 3A]. However, mtROS levels in aortic cross sections were found to be three times higher in aged LCR rats than in HCR rats [Figure 3A; $P = 0.0013$]. In agreement with this, the aortic VSMCs of old age LCR rats have a 2-fold increased mtROS level compared to that of old age HCR rats [Figure 3B; $P < 0.05$; Supplementary Figure 3], suggesting a link between low aerobic capacity and increased mitochondrial oxidative stress during old age.

Since increased mitochondrial oxidative stress can cause mtDNA damage[58,59], we investigated mtDNA integrity by long PCR amplification of a 13.4 kb mtDNA fragment. Consistent with the increase in mtROS

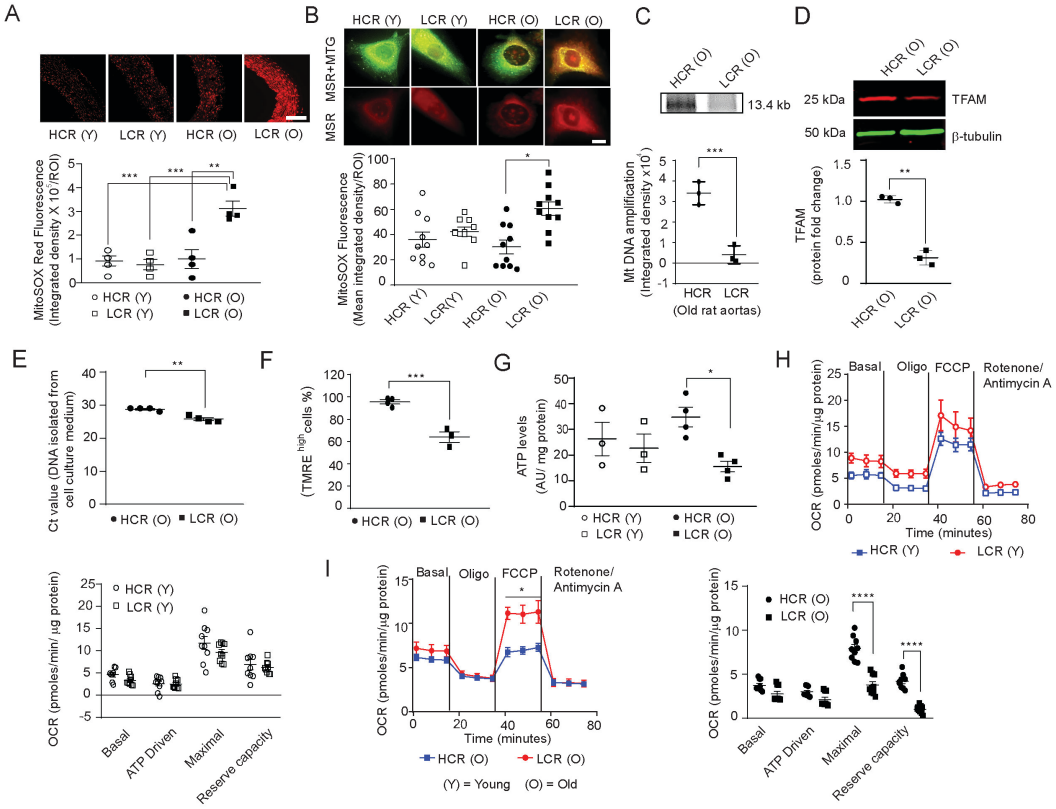

Figure 3. LCR rats show increased mitochondrial oxidative stress, mtDNA damage, circulating mitochondrial DAMPs and dysfunction in old age. Representative fluorescence images of aortic cross sections stained with MitoSOX Red (MSR) (A, top panel, scale 50 µm) and VSMCs stained with MitoTracker Green (MTG) and MitoSOX Red (B, top panel, scale 10 µm) from young and old age HCR and LCR rats. MitoSOX Red fluorescence was presented as integrated density (mean ± SEM, *n* = 4) (A and B bottom panels). Representative long PCR amplicon of 13.4 kb mitochondrial DNA from aortas (C, top panel) from old age HCR and LCR rats. PCR product band intensities were normalized to a short amplicon of 0.22 kb GAPDH (mean ± SEM, *n* = 3) (C, bottom panel). Western blot analysis and densitometric quantification of TFAM in VSMC lysates (D, top panel). Data are presented as fold change ± SEM where *n* = 4 (*D*, bottom panel). The amount of mtDNA was estimated by qPCR of cell-free DNA isolated from a fixed volume of VSMC cell-free culture medium (E). Data presented as cycle number ± SEM, *n* = 3-4. Mitochondrial membrane potential was measured by flow cytometry and the data presented as percentage of cells scored positive for high tetramethylrhodamine ethyl ester (TMRE) fluorescence. Data are mean ± SEM, *n* = 3-4 (F). ATP levels were measured using a colorimetric assay kit and the data presented are arbitrary units (mean ± SEM, *n* = 4 (G). Oxygen consumption rate (OCR) of aortic VSMCs isolated from young and old age rats. VSMCs were plated at a density of 15000 cells/well in the XF96 culture plates and OCR was measured at the basal level and in the presence of 2 µM oligomycin, 500 nM trifluoromethoxy carbonylcyanide phenylhydrazone (FCCP), and 0.5 µM antimycin A + 500 nM rotenone in VSMCs from young (H, left panel) and old age (I, left panel) LCR and HCR rats. Mitochondrial bioenergetic parameters were derived from VSMC OCR measurements (H and I, right panels). Data are mean ± SEM, *n* = 4. **P* < 0.05; ***P* < 0.01; *****P* < 0.0001.

levels, an 8.6-fold lower mtDNA amplification was observed in aortas from aged LCR rats compared to aged HCR rats [Figure 3C]. We wondered if this dramatic reduction in mtDNA amplification was due to an additive effect of mitochondrial ROS and the loss of protective mechanisms. Western analysis for TFAM in the VSMC lysates showed a 3.3-fold decrease in old LCRs compared to old HCRs [Figure 3D]. Based on these results, low aerobic capacity-induced mtROS contribute to mtDNA damage in old age, impairing the replication of mtDNA.

Because aging can lead to increased production of damage-associated molecular patterns (DAMPs)[25], we investigated the effect of the interaction of low aerobic capacity and aging on mtDNA damage as measured by QPCR with a short Taqman probe specific for MTCO1 gene amplification in VSMC culture medium of

aged LCR and HCR rats. The Ct value for MTCO1 amplification decreased significantly in DNA amplified from VSMC culture media from old age LCR rats compared with that in HCR rats, which is inversely related to the amount of extracellular MTCO1 DNA present in the culture media [> 2 Ct value decrease, $P < 0.01$, Figure 3E].

Because extrusion of cellular mtDNA occurs following mitochondrial depolarization[23], we measured mitochondrial membrane potential in rat aortic VSMCs from old age LCR and HCR rats by flow cytometric analysis of TMRE retention[60]. A 30% decrease in $TMRE^{high}$ cells was observed in old age LCR rat VSMCs compared with HCR rat cells [Figure 3F]. Mitochondrial membrane potential harnesses proton motive force to generate ATP. A colorimetric assay was used to compare levels of ATP in VSMCs from young and old age LCR and HCR rats. The VSMCs from older LCR rats exhibited 2.24-fold lower ATP levels ($P < 0.05$) than VMSCs from younger HCR rats, while cells from young LCR and HCR rats exhibited equal ATP levels [Figure 3G].

The mtDNA-encoded proteins are essential components of respiratory complex subunits, and mtDNA damage compromises cellular respiration[61]. We measured oxygen consumption rate (OCR) to examine the effects of low aerobic exercise capacity as well as aging on VSMC respiration. The OCR of VSMCs from young LCR and HCR rats was not significantly different [Figure 3H]. However, the maximal OCR by complex IV in the presence of FCCP, which collapses the proton gradient and disrupts the mitochondrial membrane potential and enables an uninhibited electron transport chain, was significantly lower in VSMCs from old age LCR compared to HCR rats [Figure 3I]. In addition, the reserve respiratory capacity, defined as the difference between maximal and basal respiration, was significantly lower in VSMCs from old age LCR versus HCR rats [Figure 3I]. Together, these data confirm that low aerobic capacity negatively affects the ability of conduit arteries in LCR rats to respond to increased energy demands or stresses, particularly as the animals age.

LCR rats exhibit impaired mitophagy in aging

Inhibition of mitophagy, the autophagy of mitochondria, causes the accumulation of dysfunctional mitochondria and extrusion of mitochondrial components[25]. As we observed increased mitochondrial damage and higher levels of mtDNA DAMPs, we investigated whether LCR rats suffer from impaired mitophagy in old age. Mitophagy was measured as integrated density from the colocalization of immunofluorescent red mitochondrial marker protein TOM20 with green lysosomal marker protein LAMP1 and blue SM α-actin in aortas and from the colocalization of red TOM20 and green LAMP1 in VSMCs. Older LCR rats displayed a 54% decrease in mitophagy in medial SMCs of aortas [Figure 4A], which was also supported by a 76% reduction in cultured VSMCs [Figure 4B; Supplementary Figure 4] in comparison to older HCR rats. The mitophagy levels did not differ significantly between young age LCR and HCR rats.

Mitophagy induction in live VMSCs was observed using Mtphagy Dye, which emits a high signal when damaged mitochondria fuse with lysosomes (Mitophagy kit, Dojindo) in the presence of rapamycin, a well-known mitophagy inducer[62]. The fusion of Mtphagy Dye-labeled mitochondria and lysosomes was confirmed with Lyso Dye. The rapamycin-induced mitophagy in VSMCs of both young and old LCR and HCR rats [Figure 4C]. However, mitophagy induction was higher in VSMCs of young HCR rats than in old LCR rats, and in VSMCs of old HCR rats than in old LCR rats.

The autophagic vacuole formation is one of the essential steps in transporting damaged mitochondria into lysosomal compartments. We measured the formation of autophagic vacuoles in VSMCs by measuring the

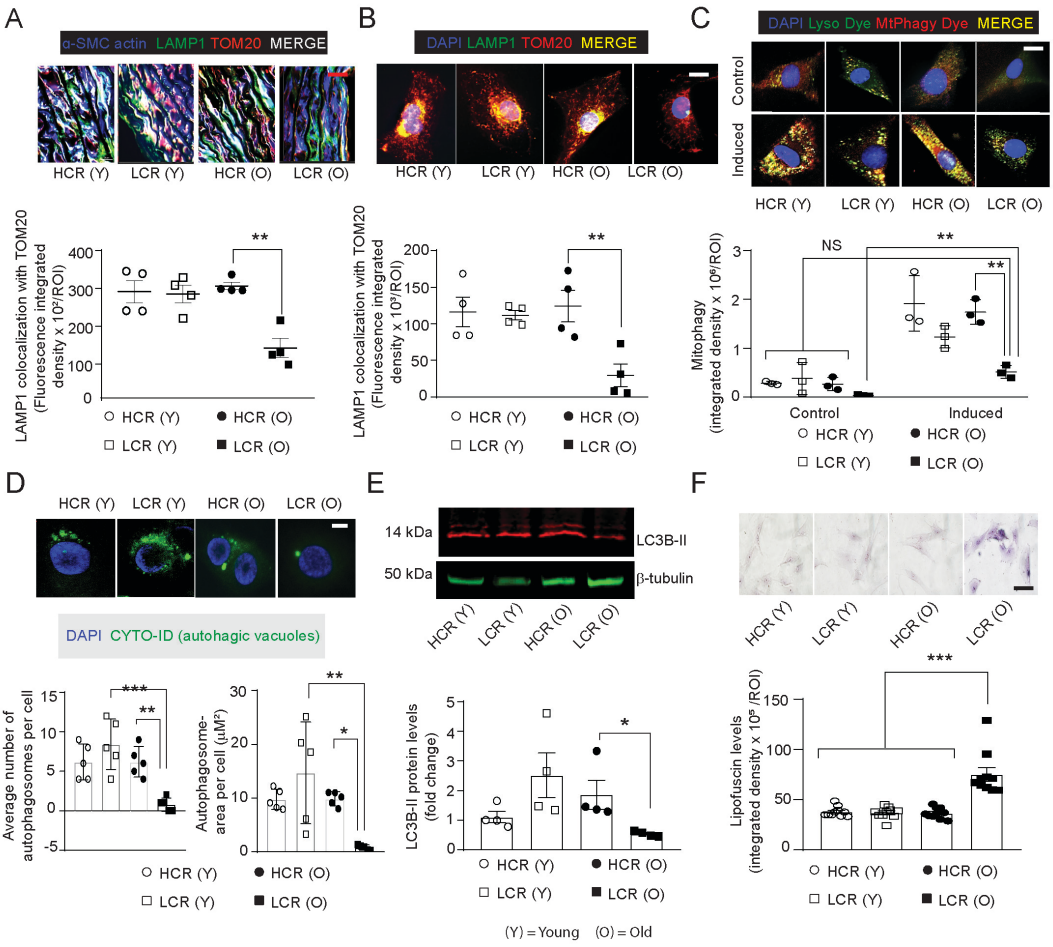

Figure 4. VSMCs of the aortic media and cultured aortic VSMCs of old age LCR rats show impaired mitophagy. Representative confocal images of aortic cross sections (A, top panel) were co-stained for LAMP1 (green), TOM20 (red) and SM-α-actin (blue). The white fluorescence indicates colocalization of all proteins and active mitophagy in medial VSMCs. VSMCs (B, top panel) were co-stained for LAMP1 (green) and TOM20 (red). Bright yellow fluorescence indicates colocalization of LAMP1 and TOM20 and active mitophagy. Data are presented as mean integrated density/ROI ± SEM where *n* = 4 independent cell lines (A and B, bottom panels). Representative confocal images of mitophagy flux, showing bright yellow colocalization of Mtphagy-(red) and Lyso-(green) dyes (C, top panel; scale 10 μm). Data are mean integrated density/ROI ± SEM. Representative images of autophagic vacuole formation were measured by the green fluorescence puncta of a specific dye, CYTO-ID (ENZO) (D, top panel; scale 10 μm). Data are the average number of punctate vacuolar structures per cell (number) or the average pixel area of fluorescence integrated density/ROI ± SEM (D, bottom panel). Western blot analysis and densitometric quantification of mitophagy/autophagy marker LC3B in VSMC lysates (E). Data are mean ± SEM where *n* = 4. Representative immunohistochemistry images of VSMC stained with Sudan Black B (F, top panel; scale = 50 μm). Data are presented as mean integrated density/ROI ± SEM where *n* = 4 (F, bottom panel). **P* < 0.05; ***P* < 0.01; ****P* < 0.001.

green-fluorescent puncta that form when CYTO-ID (ENZO Inc.) is specifically localized to autophagic vacuoles. In old LCR VSMCs, green fluorescence area of puncta was 12.0-fold lower than in old HCR VSMCs, indicating impaired autophagy flux, but this difference was not found in young HCR and LCR VSMCs [Figure 4D]. Western blot analysis of VSMC lysates also revealed a decreased level of LC3B-II, a marker of autophagosomes, in old LCR rats compared to old HCR rats [Figure 4E, $P < 0.05$]. Additionally, we tested the effects of autophagic flux inhibitor Bafilomycin A1 (50 nM for 16 h) on LC3B-II and autophagic adapter p62 levels in VSMCs. The levels of p62 [Supplementary Figure 5A] and LC3B-II [Supplementary Figure 5B] in VSMCs from young LCR and HCR rats as well as old HCR rats were significantly increased by bafilomycin A1. In contrast, p62 and LC3B-II levels in VSMCs from old LCR rats were lower than those from old HCR rats, indicating lower synthesis of these proteins and impaired

autophagy and mitophagy. The results of Western blot analysis failed to show differences between VSMCs from old LCR and HCR rats in p62 or LC3B-II levels in response to Bafilomycin A1 treatment, possibly due to heterogeneity of HCR/LCR rats and difference in the sensitivity of the assays [Supplementary Figure 5C]. Additionally, the accumulation of lipofuscin, an indicator of lysosomal dysfunction and a biomarker of impaired molecular and organellar recycling, was significantly greater in VSMCs of old LCR rats compared with those of old HCR rats [Figure 4F, $P < 0.05$]. Based on these findings, it appears impaired autophagy/mitophagy underlies mitochondrial dysfunction with aging in LCR rats.

Inflammasome activation in aging is associated with diminished aerobic capacity

The inhibition of mitophagy activates inflammasomes, cytosolic danger sensing platforms via increased mitochondrial ROS generation and DAMPs[27,63]. Damaged mtDNA is actively extruded from cells via exosomes, and cytosolic DNA activates the AIM2 inflammasome[64]. Hence, we investigated whether impaired mitophagy and elevated DAMP levels in old LCR rat VSMCs increase the expression of AIM2, caspase-1 and IL-18, which are downstream effectors of AIM2 inflammasome activation. As shown in Figure 5A, immunofluorescence studies indicated a marked increase in AIM2 (4.1-fold), caspase-1 (5.6-fold), and IL-18 expression (18.3-fold) within the medial layer of aortic cross sections from old age LCR rats compared with HCR rats.

In consonance with inflammasome activation, VCAM-1, a major regulator of leukocyte adhesion and transendothelial migration that is upregulated in chronic inflammatory conditions[65], also increased by 40-fold in old age LCR rat aortic medial layer compared with HCR rats [Figure 5A]. Using Western blotting, we investigated the expression of AIM2 and its downstream effectors in aortic VSMC lysates in order to corroborate inflammasome expression and activation in aortic media at the intersection between aging and low oxidative capacity. Similar to the findings of aortic immunofluorescence, the expression levels of AIM2, IL-18, and cleaved caspase-1 were 3.0, 2.0, and 1.8-fold greater, respectively, in aged LCR rat VMSCs compared to HCR rat VSMCs [Figure 5B, Supplementary Figure 6A]. VCAM-1 expression increased 1.9-fold in aged LCR rat VMSCs compared to aged HCR rat cells, confirming increased inflammation [Figure 5B]. The levels of inflammasome expression/activity or effector protein expression were not significantly different between the young LCR and HCR rat aortas [Figure 5A] or VMSC lysates [Figure 5B]. In addition, we examined NLRP3 inflammasome expression in young and old rat aortic VSMCs. No significant differences in NLRP3 protein levels were observed between young and old LCR and HCR rat aortic VSMC lysates [Supplementary Figure 6B].

Rapamycin and MitoTEMPO attenuate inflammasome activation in aortic VSMCs from old age LCR rats

To determine whether mtDNA damage is sufficient to induce inflammasome expression and activation, VSMCs from young LCR rats were treated with liver mtDNA DAMPs at a concentration of 10 ng/mL for 24 h. The levels of inflammasome expression and activation markers in VSMCs treated with DAMPs were comparable to those in untreated VSMCs from old age LCR rats, and DAMP treatment increased AIM2, cleaved caspase-1, and cleaved IL-18 levels by 18.6, 3.3, and 9.9-fold, respectively [Figure 6A and B, Supplementary Figure 7A]. The high degree of variability in inflammasome marker expression in response to DAMPs treatment might reflect the polygenic backgrounds of rat strains.

Since rapamycin inhibits AIM2 activation[66] and reduces aortic stiffness with aging[67], we investigated whether rapamycin inhibits AIM2 pathway activation in aged LCR rat VSMCs. Rapamycin decreased cleaved caspase-1 and cleaved IL-18 levels by 2 and 7.5-fold, respectively [Figure 6C and D, Supplementary Figure 7B]. However, rapamycin had no effect on AIM2 protein levels, suggesting that inhibition occurs at the activity level rather than at the protein level. We also studied the effects of

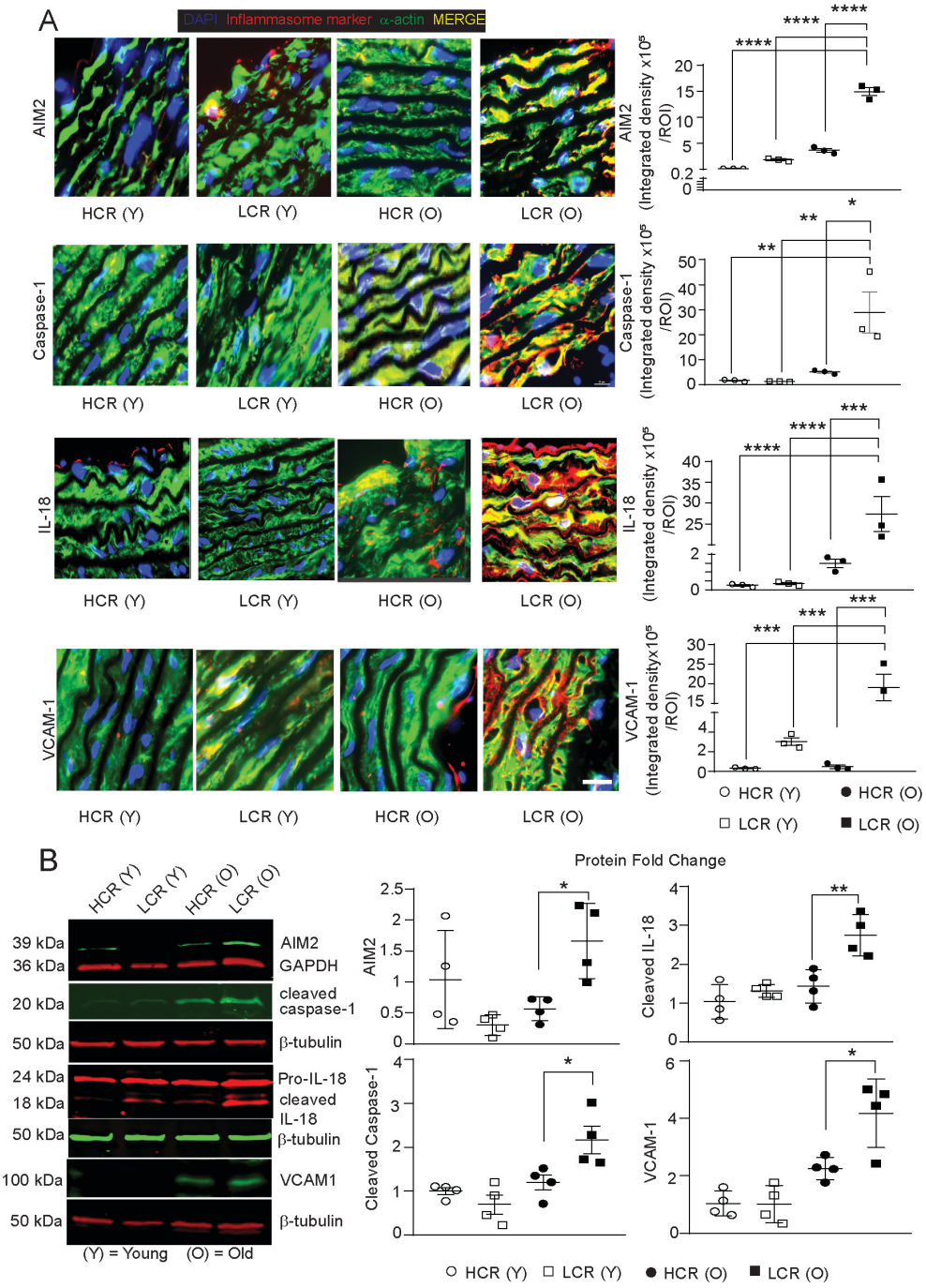

Figure 5. Inflammasome is activated in aortic medial VSMCs and in cultured aortic VSMCs of old age LCR rats. Representative confocal images of aortic cross sections stained for inflammasome activation markers (AIM2, caspase-1, IL-18, and VCAM1) in young and old age rats (A, left panels, red). Aortas were co-stained for ACTA2 (green). The bright yellow fluorescence indicates activation of specific inflammasome markers in medial VSMCs. Data are presented as average integrated density/ROI ± SEM where $n = 4$ (A, right panels). Representative Western blots showing expression of the inflammasome markers in VSMC lysates (B, left panel). Data are presented as fold change, mean ± SEM, $n = 4$ (B). Scale is 50 μm. $^{*}P < 0.05$; $^{**}P < 0.01$; $^{***}P < 0.001$.

MitoTEMPO, a mitochondria-targeted superoxide dismutase mimetic[20], on AIM2 pathway activation in VSMCs from old LCR rats. MitoTEMPO decreased the levels of cleaved caspase-1 and IL-18 levels by 7.6

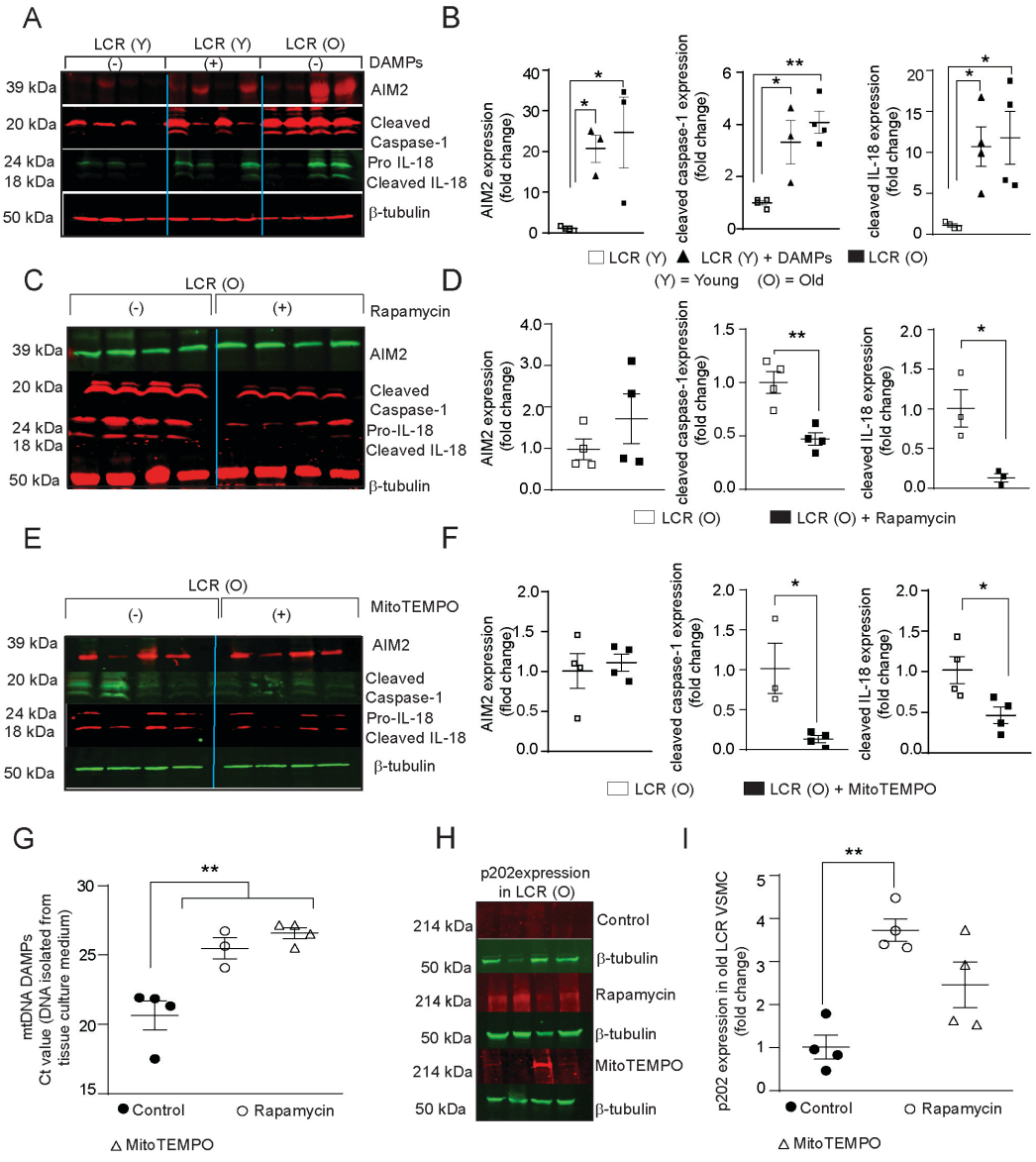

Figure 6. Rapamycin or MitoTEMPO treatment inhibited inflammasome activation in VSMCs from old LCR rats. Representative Western blots of inflammasome marker proteins of VSMCs treated with or without DAMPs (A). Densitometric quantification of proteins expressed as fold change ± SEM, *n* = 4 independent cell lines (B). Representative Western blots of inflammasome markers in VSMC lysates were isolated after 16 h of 20 nM rapamycin treatment (C). Densitometric quantification of protein levels expressed as fold change ± SEM, *n* = 4 (D). Representative Western blots of inflammasome markers in VSMC lysates after 16 h of 10 nM MitoTEMPO treatment (E). Densitometric quantification of protein levels expressed as fold change ± SEM, *n* = 4 (F). Estimation of circulating mitochondrial DNA with MTCO1 specific-Taqman probe using qPCR. Data are Ct values (Mean ± SEM, *n* = 3-4) (G). Representative Western blots of p202 protein levels in VSMC lysates with and without rapamycin or MitoTEMPO treatments (H). Densitometric quantification of protein levels expressed as fold change ± SEM, *n* = 4. (I). **P* < 0.05; ***P* < 0.01.

and 2.2-fold, respectively [Figure 6E and F, Supplementary Figure 7C]. However, MitoTEMPO did not affect AIM2 expression levels.

Next, we tested whether inhibition of inflammasome activation resulted from decreased mtDNA DAMP generation. From rapamycin-treated and untreated VSMC culture media, cell-free DNA was isolated and mtDNA DAMP levels were determined by analyzing the MTCO1 gene by quantitative PCR. The rapamycin

treatment reduced mtDNA amplification by 4.5 ± 1.7 cycles ($P < 0.05$) [Figure 6G]. MitoTEMPO also reduced mtDNA DAMP levels in the culture medium of old age LCR rats [Figure 6G], supporting the notion that inflammasome activation increases mtDNA DAMPS levels, exacerbating inflammation in a feedforward manner.

The hematopoietic interferon-inducible nuclear protein p202 serves as a dominant-negative antagonist of AIM2, blocking downstream signal transduction by binding to cytoplasmic dsDNA that act as ligands to AIM2[68]. Because none of the antagonists we tested had an effect on AIM2 protein expression, we examined p202 levels in response to antagonist treatment in VSMCs from old LCR rats. Rapamycin increased p202 levels by 3.7-fold [Figure 6H and I]. MitoTEMPO increased p202 levels 2.4-fold, but the effect was not statistically significant. Together, these data support the notion that targeting mtDNA damage and decreasing mtDNA DAMPs prevents inflammasome activation at the intersection of low oxidative capacity and aging.

Rapamycin and MitoTEMPO reduced mitochondrial oxidative stress and increased mitophagy and OCR in VSMCs from old LCR rats

We next examined whether rapamycin or MitoTEMPO had salutary effects on mitophagy. Both rapamycin and MitoTEMPO increased mitophagy by 4.8 and 2.9-fold over respective controls, as measured by colocalization of LAMP1 with TOM20 [Figure 7A and B; Supplementary Figure 8A]. The mitochondrial ROS levels, as assessed by changes in MitoSOX Red fluorescence, decreased by 2.5 and 3-fold in old LCR rat VSMCs treated with rapamycin and MitoTEMPO compared to respective controls [Figure 7C and D, Supplementary Figure 8B], suggesting impaired mitophagy promotes ROS generation[69]. In order to determine whether enhanced mitophagy and reduced mitochondrial ROS levels affected mitochondrial function, we measured OCR in VSMCs from old LCR rats treated with and without rapamycin and MitoTEMPO. Both the compounds significantly increased maximal OCR and reserve respiratory capacity in old LCR rat VSMCs [Figure 7E-H], suggesting the importance of mitochondrial function in vascular health at the intersection of aging and low oxidative capacity.

DISCUSSION

In the present study, we provide experimental evidence that mtDNA damage and dysfunction are induced by low intrinsic aerobic capacity and aging, adversely affecting vascular health. Our results show: (1) increased transcription of genes involved in cell cycle regulation and pro-inflammatory pathways, impaired mitophagy, and impaired oxidative phosphorylation pathways in old age LCR rat aortas versus longevity regulating pathways, increased oxidative phosphorylation and mitophagy/autophagy pathways in old age HCR rat aortas; (2) impaired arterial relaxation and increased aortic stiffness in old age LCR rats compared to the HCR rats; (3) increased mitochondrial oxidative stress and DNA damage in aortas and mitochondrial oxidative stress in aortic VSMCs of old age LCR versus HCR rats; (4) increased expression of AIM2 and its downstream effectors and VCAM1 in the aortic medial layer, as well as AIM2 activation in the aortic VSMCs of old age LCR versus HCR rats; (5) mtDNA DAMP-treated VSMCs from young LCR rats show similar expression and activation of AIM2 inflammasome as do those from old LCR rats; and (6) rapamycin and MitoTEMPO attenuate mtDNA DAMPs-induced inflammasome activation in young LCR rat aortic VSMCs and reduce mitochondrial oxidative stress, improving OCR and mitophagy in old age LCR rat VSMCs. Together, these results demonstrate that mtDNA DAMPs associated with low aerobic capacity contribute to sterile inflammation in aging, resulting in vascular dysfunction and aortic stiffness.

We and others have demonstrated that increased mitochondrial oxidative stress in aging causes arterial stiffening[16,30,40,55]. Seals and colleagues reported that mitochondrial quality control, a balance between

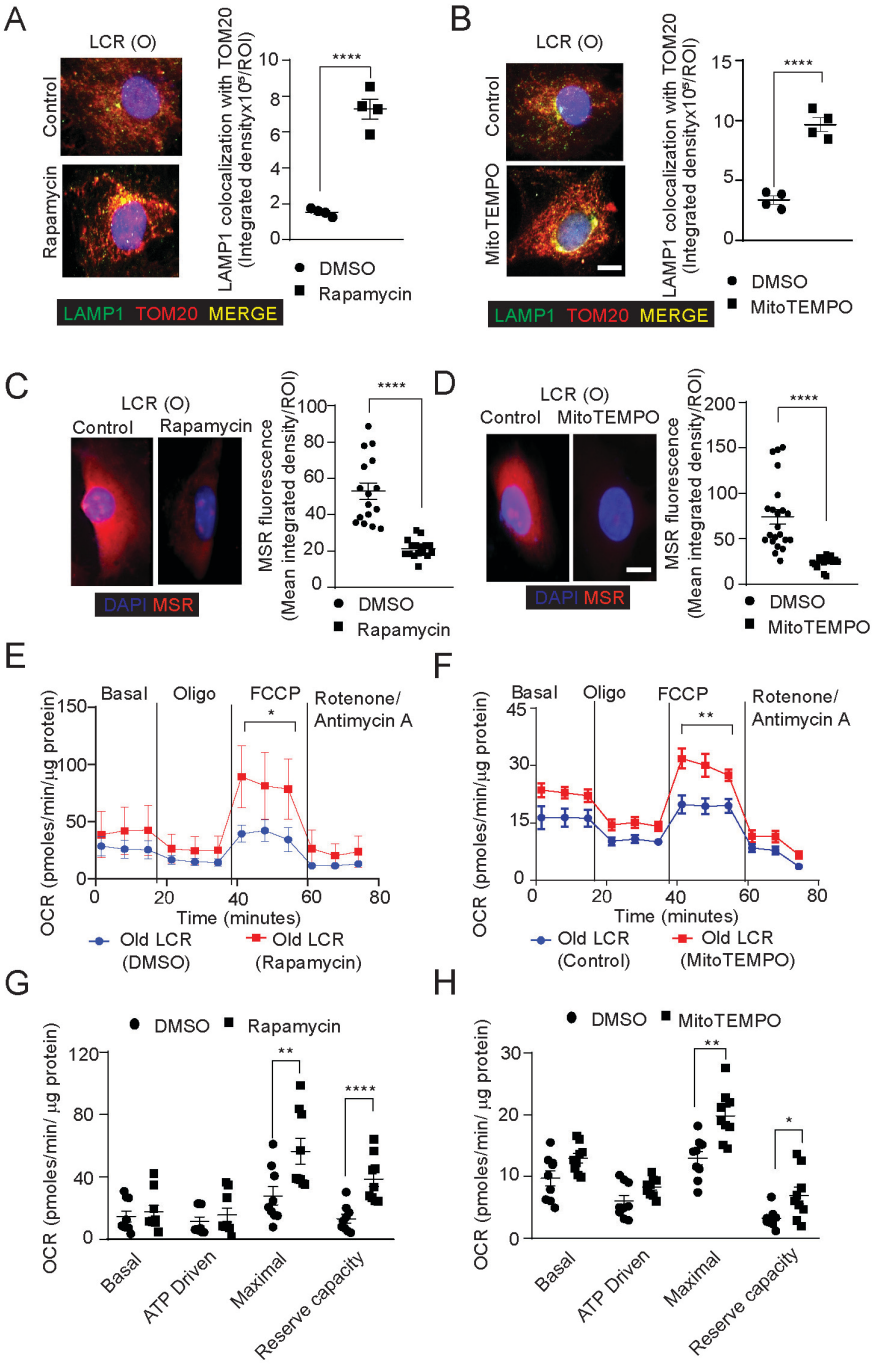

Figure 7. Treatment with rapamycin or MitoTEMPO decreases oxidative stress and enhances mitophagy and OCR in old age LCR rat VSMCs. Representative confocal images of VSMCs treated with and without 20 nM rapamycin (A), or MitoTEMPO (B) and co-stained for lysosomal marker LAMP1 (green) and mitochondrial marker TOM20 (red). Bright yellow fluorescence indicates colocalization of LAMP1 and TOM20 and active mitophagy. Data are presented as average integrated density/ROI ± SEM where $n = 4$. Scale is 10 µm. Representative confocal images of mitochondrial ROS levels with and without rapamycin (C) or MitoTEMPO (D) treatments as measured by MitoSOX Red (MSR) fluorescence. Intensity of fluorescence was presented as integrated density (mean ± SEM, $n = 4$, Scale is 10 µm). OCR was measured at the basal level and in the presence of 2 µM oligomycin, 500 nM trifluoromethoxy carbonylcyanide phenylhydrazone (FCCP), and 0.5 µM antimycin A + 500 nM rotenone in VMSCs of old age LCR rats treated without and with rapamycin (E and G) or MitoTEMPO (F and H). Mitochondrial bioenergetic parameters were derived from VSMC OCR measurements.

mitochondrial biogenesis and mitophagy, is impaired in aging, resulting in higher collagen-1 levels and aortic stiffness[30]. The present data demonstrate that mitochondrial oxidative stress causes VSMC and arterial dysfunction, as evidenced by impaired relaxation of the mesenteric arteries to acetylcholine and aortic stiffening in older LCR rats, extracellular matrix remodeling and fibrosis, and by a leftward shift in the stress-strain curves. The increased production of mitochondrial ROS and inflammation, as evident by increased IL-18 and VCAM1 levels in VSMCs old LCR rats, causes oxidative damage and degradation of elastic laminae, as well as excessive collagen deposition in the vascular wall. Increased vascular stiffness and dysfunction are a direct consequence of these processes[40]. Endothelial dysfunction resulting from increased mitochondrial oxidative stress may also contribute to aortic stiffening in old age LCR rats, as illustrated by decreased eNOS levels, decreased phosphorylation of eNOS (Ser1177), and TGF-β1 upregulation in aortic medial VSMCs induced by eNOS inhibition[49,53,70]. Several mechanisms may have contributed to the downregulation of eNOS in old LCR rats. First, LCR rats exhibit a phenotype of metabolic syndrome, including obesity[71] which is associated with decreased levels of eNOS[72,73]. Second, TNF-α, which is increased in obesity, was shown to downregulate eNOS expression[73]. Interestingly, TNF-α levels were higher in the media of cultured LCR splenic mononuclear cells[74], suggesting that TNF-α may downregulate eNOS in LCR rats. Lastly, mitochondrial abnormalities due to oxidative stress may have decreased eNOS expression[70] and our data indicate elevated mitochondrial ROS in LCR vasculature.

Reduced cardiorespiratory fitness is associated with arterial stiffness in coronary artery disease patients[33]. Chronic exercise training in aged rats reduces mitochondrial ROS production, preserving aortic mitochondrial function, and reducing aortic stiffening[75]. Old age HCR rats that demonstrate better mitochondrial energetics, lower ROS levels and less DNA damage in VSMCs than do age-matched LCR rats are protected against aortic stiffening and arterial dysfunction. These results are in general agreement with a study in which cardiomyocytes from HCR rats showed higher aerobic capacity, mitochondrial fitness, and health in association with a longer lifespan[76].

Moreover, our data indicating impaired autophagy and lysosomal dysfunction in aortic VSMCs in old age LCR rats agree with the reports of age-associated decline in proteolytic systems involved in protein quality control, including the autophagy-lysosomal system[77,78]. Aged LCR rats have a significant increase in mitochondrial ROS levels, mtDNA damage and nuclear DNA damage compared with young LCR rats. It is suggested that impaired mitophagy may be caused by reduced ATP levels that inhibit lysosomal function and protein sequestration[79]. When mitochondrial depolarization occurs, PINK1 recruits Parkin to mitochondria and initiates mitophagy. Mitophagy could be compromised by low levels of ATP, which inhibits the upregulation of PINK1 levels and the recruitment of Parkin into mitochondria[80]. As mitophagy genes are encoded by nuclear DNA, impaired mitophagy may reflect nuclear DNA damage in aged LCR rats[81].

Perhaps lower mitochondrial ROS levels and less nuclear and mtDNA damage can explain why mitophagy is not impaired in aged HCR rats. In fact, our RNA-Seq data show upregulation of mitophagy in old HCR rats. In addition, insulin signaling[82] and AMPK signaling[83,84] pathways that are implicated in mitophagy activation are upregulated in old HCR rats. Further supporting impaired mitophagy in old LCR rats, mitochondrial quality control and biogenesis effectors SIRT1/TFAM are downregulated in aged LCR rats[85], whereas SIRT3 levels in SIRT3/FOXO3A-PINK1-PARKIN axis[86] linked to higher mitophagy are high in HCR rats[87].

Additionally, our findings are also supported by the observation that autophagy/mitophagy and mitochondrial fitness are better preserved in HCR rats compared to LCR rats[76]. An impaired mitophagy,

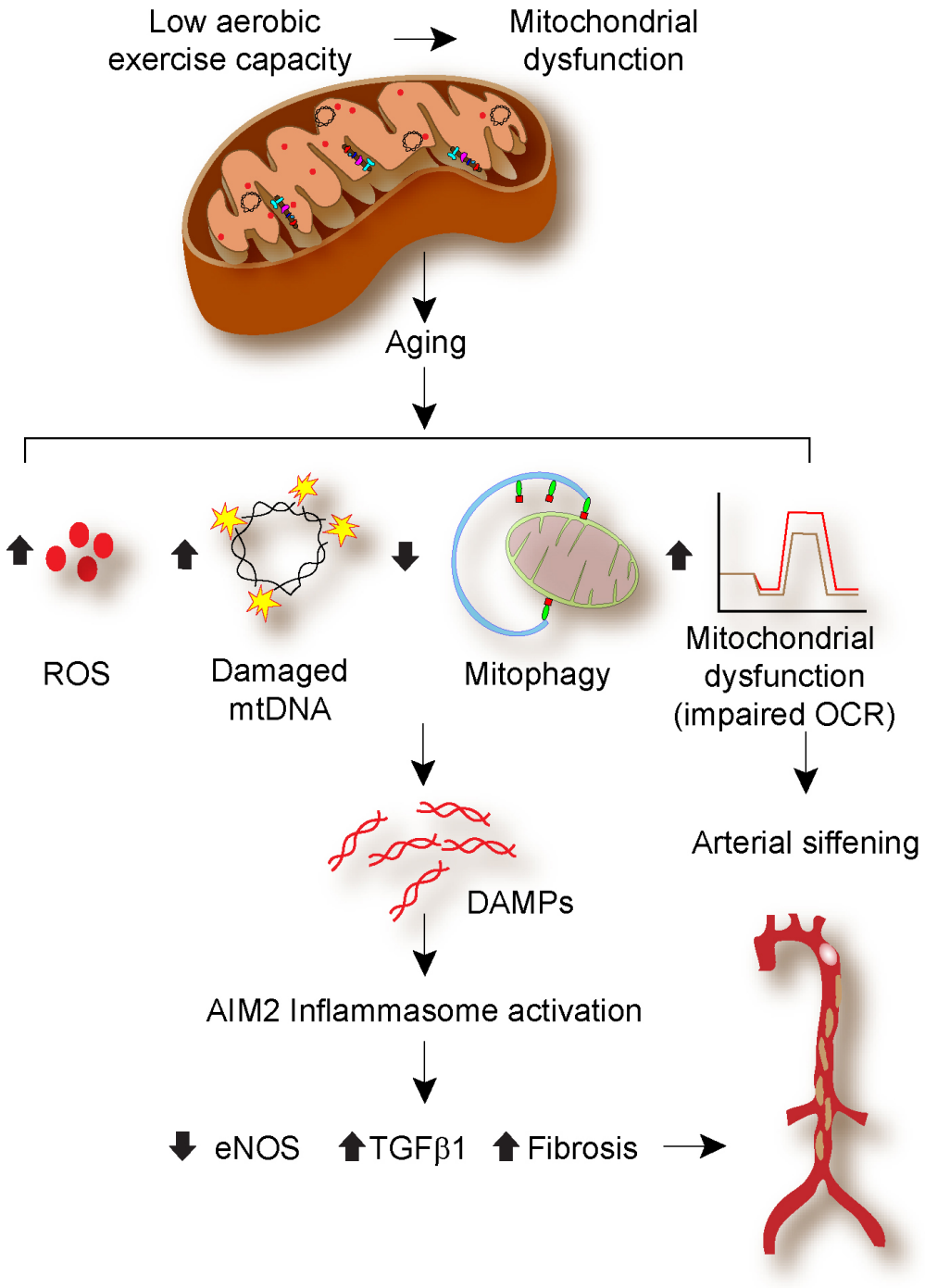

Figure 8. Schematic representation of the low aerobic capacity and aging leading to arterial stiffening.

especially in a context of pronounced energy deficits, such as in the LCR rat aortas, causes an accumulation of fragments of the mitochondrial genome, such as DAMPs, resulting in sterile inflammation[88]. In fact, higher DAMP levels in aging have been proposed as a potential mechanism for inflammaging[89]. As per conventional wisdom, various pathways of mitochondrial dysfunction converge to activate NLRP3 inflammasomes, but not other types of inflammasomes[90,91]. In contrast, our results indicate higher AIM2 protein levels and AIM2 inflammasome activation in aortic medial VSMCs and isolated aortic VSMCs of

old age LCR rats. Interestingly, AIM2 protein expression as well as AIM2 inflammasome activity were both increased in young LCR aortic VSMCs treated with mtDNA DAMPs in culture, supporting the notion that mtDNA DAMPs are inflammaging inducers.

Both rapamycin and MitoTEMPO inhibited AIM2 inflammasome activation but did not inhibit its expression. Rapamycin can reverse age-related vascular dysfunction and increase longevity in rodents[67]. The inhibitory effect of rapamycin[64] on AIM2 activation was attributed to their autophagy/mitophagy-promoting actions. Interestingly, MitoTEMPO was able to inhibit mtDNA DAMP-induced AIM2 inflammasome activity and rescue mitophagy, perhaps by reducing mtROS levels. Additionally, both treatments enhanced the mitochondrial respiratory capacity of VSMCs from old-age LCR rats, which might contribute to better vascular function. Furthermore, the treatments inhibited mtDNA damage in aortic VSMCs in aging, possibly disrupting the nexus between DNA damage and inflammasome activation[92]. Rapamycin increased p202 levels, which may block DAMPs binding to AIM2 inflammasomes[68]. These findings are supported by the observation that rapamycin[66] and MitoTEMPO[93] inhibit the activity of AIM2 inflammasomes. We and others have shown that rapamycin and MitoTEMPO are beneficial against aortic stiffening in mouse models of oxidative stress[40,67].

In summary, our data demonstrate that low aerobic capacity and aging cause mitochondrial dysfunction and increase mtROS levels, impair autophagy and mitophagy, resulting in increased inflammasome activation. Mitochondrial turnover in aging is intricately intertwined with inflammasome activation, affecting mitochondrial fitness, VSMC and endothelial function, and vascular health [Figure 8]. Mitophagy induction and inflammasome inhibition, as well as the use of mitochondrial antioxidants, may prove to be helpful therapeutic strategies for enhancing vascular health in older *individuals* with a reduced aerobic capacity.

DECLARATIONS

Authors' contributions

Designed the study and experiments: Canugovi C, Madamanchi NR
Performed the experiments: Canugovi C, Stevenson MD, Vendrov AE, Lozhkin A
Wrote the manuscript: Canugovi C, Britton SL, Koch LG, Runge MS, Madamanchi NR

Availability of data and materials

Data will be provided on request.

Financial support and sponsorship

None.

Conflicts of interest

Dr. Marschall Runge is a member of the Board of Directors at Eli Lilly and Company. Other authors declared that there are no conflicts of interest.

Ethical approval and consent to participate

All animal procedures were approved by the Institutional Animal Care and Use Committee of the University of Michigan (PRO00010178).

Consent for publication

Not applicable.

REFERENCES

1. Blair SN, Kampert JB, Kohl HW, et al. Influences of cardiorespiratory fitness and other precursors on cardiovascular disease and all-cause mortality in men and women. *JAMA* 1996;276:205-10. PubMed
2. Church TS, Cheng YJ, Earnest CP, et al. Exercise capacity and body composition as predictors of mortality among men with diabetes. *Diabetes Care* 2004;27:83-8. DOI PubMed
3. Gulati M, Pandey DK, Arnsdorf MF, et al. Exercise capacity and the risk of death in women: the St James Women Take Heart Project. *Circulation* 2003;108:1554-9. DOI PubMed
4. Ladenvall P, Persson CU, Mandalenakis Z, et al. Low aerobic capacity in middle-aged men associated with increased mortality rates during 45 years of follow-up. *Eur J Prev Cardiol* 2016;23:1557-64. DOI PubMed
5. Myers J, Prakash M, Froelicher V, Do D, Partington S, Atwood JE. Exercise capacity and mortality among men referred for exercise testing. *N Engl J Med* 2002;346:793-801. DOI PubMed
6. Fleg JL, Strait J. Age-associated changes in cardiovascular structure and function: a fertile milieu for future disease. *Heart Fail Rev* 2012;17:545-54.
7. Britton SL, Koch LG. Animal genetic models for complex traits of physical capacity. *Exerc Sport Sci Rev* 2001;29:7-14. DOI PubMed
8. Koch LG, Britton SL. Artificial selection for intrinsic aerobic endurance running capacity in rats. *Physiol Genomics* 2001;5:45-52. DOI PubMed
9. Koch LG, Kemi OJ, Qi N, et al. Intrinsic aerobic capacity sets a divide for aging and longevity. *Circ Res* 2011;109:1162-72. DOI PubMed PMC
10. Wisløff U, Najjar SM, Ellingsen O, et al. Cardiovascular risk factors emerge after artificial selection for low aerobic capacity. *Science* 2005;307:418-20. DOI PubMed
11. Esposito LA, Melov S, Panov A, Cottrell BA, Wallace DC. Mitochondrial disease in mouse results in increased oxidative stress. *Proc Natl Acad Sci USA* 1999;96:4820-5. DOI PubMed PMC
12. Madamanchi NR, Runge MS. Mitochondrial dysfunction in atherosclerosis. *Circ Res* 2007;100:460-73. DOI PubMed
13. Bonnard C, Durand A, Peyrol S, et al. Mitochondrial dysfunction results from oxidative stress in the skeletal muscle of diet-induced insulin-resistant mice. *J Clin Invest* 2008;118:789-800. DOI PubMed PMC
14. Yokota T, Kinugawa S, Hirabayashi K, et al. Oxidative stress in skeletal muscle impairs mitochondrial respiration and limits exercise capacity in type 2 diabetic mice. *Am J Physiol Heart Circ Physiol* 2009;297:H1069-77. DOI PubMed
15. Mercer JR, Cheng KK, Figg N, et al. DNA damage links mitochondrial dysfunction to atherosclerosis and the metabolic syndrome. *Circ Res* 2010;107:1021-31. DOI PubMed PMC
16. Canugovi C, Stevenson MD, Vendrov AE, et al. Increased mitochondrial NADPH oxidase 4 (NOX4) expression in aging is a causative factor in aortic stiffening. *Redox Biol* 2019;26:101288. DOI PubMed PMC
17. Madamanchi NR, Hakim ZS, Runge MS. Oxidative stress in atherogenesis and arterial thrombosis: the disconnect between cellular studies and clinical outcomes. *J Thromb Haemost* 2005;3:254-67. DOI PubMed
18. Maynard S, Fang EF, Scheibye-Knudsen M, Croteau DL, Bohr VA. DNA damage, DNA repair, aging, and neurodegeneration. *Cold Spring Harb Perspect Med* 2015;5:a025130. DOI PubMed PMC
19. Moon SK, Thompson LJ, Madamanchi N, et al. Aging, oxidative responses, and proliferative capacity in cultured mouse aortic smooth muscle cells. *Am J Physiol Heart Circ Physiol* 2001;280:H2779-88. DOI PubMed
20. Vendrov AE, Stevenson MD, Alahari S, et al. Attenuated superoxide dismutase 2 activity induces atherosclerotic plaque instability during aging in hyperlipidemic mice. *J Am Heart Assoc* 2017;6:e006775. DOI PubMed PMC
21. Lemasters JJ. Selective mitochondrial autophagy, or mitophagy, as a targeted defense against oxidative stress, mitochondrial dysfunction, and aging. *Rejuvenation Res* 2005;8:3-5. DOI PubMed
22. Kubli DA, Gustafsson ÅB. Mitochondria and mitophagy: the yin and yang of cell death control. *Circ Res* 2012;111:1208-21. DOI PubMed PMC
23. Caielli S, Athale S, Domic B, et al. Oxidized mitochondrial nucleoids released by neutrophils drive type I interferon production in human lupus. *J Exp Med* 2016;213:697-713. DOI PubMed PMC
24. Choudhuri S, Chowdhury IH, Garg NJ. Mitochondrial regulation of macrophage response against pathogens. *Front Immunol* 2020;11:622602. DOI PubMed PMC
25. Picca A, Lezza AMS, Leeuwenburgh C, et al. Circulating mitochondrial DNA at the crossroads of mitochondrial dysfunction and inflammation during aging and muscle wasting disorders. *Rejuvenation Res* 2018;21:350-9. DOI PubMed PMC
26. Picca A, Lezza AMS, Leeuwenburgh C, et al. Fueling inflamm-aging through mitochondrial dysfunction: mechanisms and molecular targets. *Int J Mol Sci* 2017;18:933. DOI PubMed PMC
27. Kapetanovic R, Bokil NJ, Sweet MJ. Innate immune perturbations, accumulating DAMPs and inflammasome dysregulation: a ticking time bomb in ageing. *Ageing Res Rev* 2015;24:40-53. DOI PubMed
28. Jheng HF, Tsai PJ, Guo SM, et al. Mitochondrial fission contributes to mitochondrial dysfunction and insulin resistance in skeletal

muscle. *Mol Cell Biol* 2012;32:309-19. DOI PubMed PMC
29. Marseglia L, Manti S, D'Angelo G, et al. Oxidative stress in obesity: a critical component in human diseases. *Int J Mol Sci* 2014;16:378-400. DOI PubMed PMC
30. LaRocca TJ, Hearon CM Jr, Henson GD, Seals DR. Mitochondrial quality control and age-associated arterial stiffening. *Exp Gerontol* 2014;58:78-82. DOI PubMed PMC
31. Zanoli L, Briet M, Empana JP, et al. Vascular consequences of inflammation: a position statement from the ESH Working Group on Vascular Structure and Function and the ARTERY Society. *J Hypertens* 2020;38:1682-98. DOI PubMed PMC
32. Lakatta EG, Levy D. Arterial and cardiac aging: major shareholders in cardiovascular disease enterprises: part I: aging arteries: a "set up" for vascular disease. *Circulation* 2003;107:139-46. DOI PubMed
33. Alves AJ, Oliveira NL, Lopes S, et al. Arterial stiffness is related to impaired exercise capacity in patients with coronary artery disease and history of myocardial infarction. *Heart Lung Circ* 2019;28:1614-21. DOI PubMed
34. Vaitkevicius PV, Fleg JL, Engel JH, et al. Effects of age and aerobic capacity on arterial stiffness in healthy adults. *Circulation* 1993;88:1456-62. DOI PubMed
35. Aroor AR, Jia G, Sowers JR. Cellular mechanisms underlying obesity-induced arterial stiffness. *Am J Physiol Regul Integr Comp Physiol* 2018;314:R387-98. DOI PubMed PMC
36. Bender SB, Castorena-Gonzalez JA, Garro M, et al. Regional variation in arterial stiffening and dysfunction in Western diet-induced obesity. *Am J Physiol Heart Circ Physiol* 2015;309:H574-82. DOI PubMed PMC
37. Trapnell C, Pachter L, Salzberg SL. TopHat: discovering splice junctions with RNA-Seq. *Bioinformatics* 2009;25:1105-11. DOI PubMed PMC
38. Ge SX, Son EW, Yao R. iDEP: an integrated web application for differential expression and pathway analysis of RNA-Seq data. *BMC Bioinform* 2018;19:534. DOI PubMed PMC
39. Raudvere U, Kolberg L, Kuzmin I, et al. g:Profiler: a web server for functional enrichment analysis and conversions of gene lists (2019 update). *Nucleic Acids Res* 2019;47:W191-8. DOI PubMed PMC
40. Vendrov AE, Vendrov KC, Smith A, et al. NOX4 NADPH oxidase-dependent mitochondrial oxidative stress in aging-associated cardiovascular disease. *Antioxid Redox Signal* 2015;23:1389-409. DOI PubMed PMC
41. Akula S, Brosch IK, Leipzig ND. Fluorinated methacrylamide chitosan hydrogels enhance cellular wound healing processes. *Ann Biomed Eng* 2017;45:2693-702. DOI PubMed PMC
42. Santos JH, Meyer JN, Mandavilli BS, Houten B. Quantitative PCR-based measurement of nuclear and mitochondrial DNA damage and repair in mammalian cells. In: Henderson DS, editor. DNA Repair Protocols. Humana Press: Totowa. 2006. pp. 183-99. DOI PubMed
43. Arribas SM, Briones AM, Bellingham C, et al. Heightened aberrant deposition of hard-wearing elastin in conduit arteries of prehypertensive SHR is associated with increased stiffness and inward remodeling. *Am J Physiol Heart Circ Physiol* 2008;295:H2299-307. DOI PubMed
44. Gutiérrez-Arzapalo PY, Rodríguez-Rodríguez P, Ramiro-Cortijo D, et al. Role of fetal nutrient restriction and postnatal catch-up growth on structural and mechanical alterations of rat aorta. *J Physiol* 2018;596:5791-806. DOI PubMed PMC
45. Laurent S, Boutouyrie P, Asmar R, et al. Aortic stiffness is an independent predictor of all-cause and cardiovascular mortality in hypertensive patients. *Hypertension* 2001;37:1236-41. DOI PubMed
46. Sutton-Tyrrell K, Najjar SS, Boudreau RM, et al. Elevated aortic pulse wave velocity, a marker of arterial stiffness, predicts cardiovascular events in well-functioning older adults. *Circulation* 2005;111:3384-90. DOI PubMed
47. Mitchell GF, Hwang SJ, Vasan RS, et al. Arterial stiffness and cardiovascular events: the framingham heart study. *Circulation* 2010;121:505-11. DOI PubMed PMC
48. Soucy KG, Ryoo S, Benjo A, et al. Impaired shear stress-induced nitric oxide production through decreased NOS phosphorylation contributes to age-related vascular stiffness. *J Appl Physiol* 2006;101:1751-9. DOI PubMed
49. Fleenor BS, Marshall KD, Durrant JR, Lesniewski LA, Seals DR. Arterial stiffening with ageing is associated with transforming growth factor-β1-related changes in adventitial collagen: reversal by aerobic exercise. *J Physiol* 2010;588:3971-82. DOI PubMed PMC
50. Zieman SJ, Melenovsky V, Kass DA. Mechanisms, pathophysiology, and therapy of arterial stiffness. *Arterioscler Thromb Vasc Biol* 2005;25:932-43. DOI PubMed
51. Saura M, Zaragoza C, Herranz B, et al. Nitric oxide regulates transforming growth factor-beta signaling in endothelial cells. *Circ Res* 2005;97:1115-23. DOI PubMed
52. Crosas-Molist E, Meirelles T, López-Luque J, et al. Vascular smooth muscle cell phenotypic changes in patients with Marfan syndrome. *Arterioscler Thromb Vasc Biol* 2015;35:960-72. DOI PubMed
53. Gioscia-Ryan RA, Battson ML, Cuevas LM, Eng JS, Murphy MP, Seals DR. Mitochondria-targeted antioxidant therapy with MitoQ ameliorates aortic stiffening in old mice. *J Appl Physiol* 2018;124:1194-202. DOI PubMed PMC
54. Rossman MJ, Santos-Parker JR, Steward CAC, et al. Chronic supplementation with a mitochondrial antioxidant (MitoQ) improves vascular function in healthy older adults. *Hypertension* 2018;71:1056-63. DOI PubMed PMC
55. Zhou RH, Vendrov AE, Tchivilev I, et al. Mitochondrial oxidative stress in aortic stiffening with age: the role of smooth muscle cell function. *Arterioscler Thromb Vasc Biol* 2012;32:745-55. DOI PubMed PMC
56. Lacolley P, Regnault V, Nicoletti A, Li Z, Michel JB. The vascular smooth muscle cell in arterial pathology: a cell that can take on

multiple roles. *Cardiovasc Res* 2012;95:194-204. DOI PubMed

57. Owens GK, Kumar MS, Wamhoff BR. Molecular regulation of vascular smooth muscle cell differentiation in development and disease. *Physiol Rev* 2004;84:767-801. DOI PubMed
58. Ballinger SW, Patterson C, Knight-Lozano CA, et al. Mitochondrial integrity and function in atherogenesis. *Circulation* 2002;106:544-9. DOI PubMed
59. Wenzel P, Schuhmacher S, Kienhöfer J, et al. Manganese superoxide dismutase and aldehyde dehydrogenase deficiency increase mitochondrial oxidative stress and aggravate age-dependent vascular dysfunction. *Cardiovasc Res* 2008;80:280-9. DOI PubMed PMC
60. Crowley LC, Christensen ME, Waterhouse NJ. Measuring mitochondrial transmembrane potential by TMRE staining. *Cold Spring Harb Protoc* 2016;2016:pdb.prot087361. DOI PubMed
61. Stuart JA, Brown MF. Mitochondrial DNA maintenance and bioenergetics. *Biochim Biophys Acta* 2006;1757:79-89. DOI PubMed
62. Iwashita H, Torii S, Nagahora N, et al. Live cell imaging of mitochondrial autophagy with a novel fluorescent small molecule. *ACS Chem Biol* 2017;12:2546-51. DOI PubMed
63. Dai J, Zhang X, Li L, Chen H, Chai Y. Autophagy inhibition contributes to ROS-producing NLRP3-dependent inflammasome activation and cytokine secretion in high glucose-induced macrophages. *Cell Physiol Biochem* 2017;43:247-56. DOI PubMed
64. Ponomareva L, Liu H, Duan X, et al. AIM2, an IFN-inducible cytosolic DNA sensor, in the development of benign prostate hyperplasia and prostate cancer. *Mol Cancer Res* 2013;11:1193-202. DOI PubMed
65. Kong DH, Kim YK, Kim MR, Jang JH, Lee S. Emerging roles of vascular cell adhesion molecule-1 (VCAM-1) in immunological disorders and cancer. *Int J Mol Sci* 2018;19:1057. DOI PubMed PMC
66. Wang Y, Li Z, Teng M, Liu J. Dihydroartemisinin inhibits activation of the AIM2 inflammasome pathway and NF-κB/HIF-1α/VEGF pathway by inducing autophagy in A431 human cutaneous squamous cell carcinoma cells. *Int J Med Sci* 2021;18:2705-15. DOI PubMed PMC
67. Lesniewski LA, Seals DR, Walker AE, et al. Dietary rapamycin supplementation reverses age-related vascular dysfunction and oxidative stress, while modulating nutrient-sensing, cell cycle, and senescence pathways. *Aging Cell* 2017;16:17-26. DOI PubMed PMC
68. Ru H, Ni X, Zhao L, et al. Structural basis for termination of AIM2-mediated signaling by p202. *Cell Res* 2013;23:855-8. DOI PubMed PMC
69. Linton PJ, Gurney M, Sengstock D, Mentzer RM Jr, Gottlieb RA. This old heart: cardiac aging and autophagy. *J Mol Cell Cardiol* 2015;83:44-54. DOI PubMed PMC
70. Kahveci AS, Barnatan TT, Kahveci A, et al. Oxidative stress and mitochondrial abnormalities contribute to decreased endothelial nitric oxide synthase expression and renal disease progression in early experimental polycystic kidney disease. *Int J Mol Sci* 2020;21:1994. DOI PubMed PMC
71. Morris EM, Meers GME, Ruegsegger GN, et al. Intrinsic high aerobic capacity in male rats protects against diet-induced insulin resistance. *Endocrinology* 2019;160:1179-92. DOI PubMed PMC
72. Sansbury BE, Cummins TD, Tang Y, et al. Overexpression of endothelial nitric oxide synthase prevents diet-induced obesity and regulates adipocyte phenotype. *Circ Res* 2012;111:1176-89. DOI PubMed PMC
73. Valerio A, Cardile A, Cozzi V, et al. TNF-α downregulates eNOS expression and mitochondrial biogenesis in fat and muscle of obese rodents. *J Clin Invest* 2006;116:2791-8. DOI PubMed PMC
74. Su X, Feng X, Terrando N, et al. Dysfunction of inflammation-resolving pathways is associated with exaggerated postoperative cognitive decline in a rat model of the metabolic syndrome. *Mol Med* 2013;18:1481-90. DOI PubMed PMC
75. Gu Q, Wang B, Zhang XF, Ma YP, Liu JD, Wang XZ. Chronic aerobic exercise training attenuates aortic stiffening and endothelial dysfunction through preserving aortic mitochondrial function in aged rats. *Exp Gerontol* 2014;56:37-44. DOI PubMed
76. Aon MA, Cortassa S, Juhaszova M, et al. Mitochondrial health is enhanced in rats with higher vs. lower intrinsic exercise capacity and extended lifespan. *NPJ Aging Mech Dis* 2021;7:1. DOI PubMed PMC
77. López-Otín C, Blasco MA, Partridge L, Serrano M, Kroemer G. The hallmarks of aging. *Cell* 2013;153:1194-217. DOI PubMed PMC
78. Tomaru U, Takahashi S, Ishizu A, et al. Decreased proteasomal activity causes age-related phenotypes and promotes the development of metabolic abnormalities. *Am J Pathol* 2012;180:963-72. DOI PubMed
79. Doblado L, Lueck C, Rey C, et al. Mitophagy in human diseases. *Int J Mol Sci* 2021;22:3903. DOI PubMed PMC
80. Lee S, Zhang C, Liu X. Role of glucose metabolism and ATP in maintaining PINK1 levels during Parkin-mediated mitochondrial damage responses. *J Biol Chem* 2015;290:904-17. DOI PubMed PMC
81. D'Amico D, Mottis A, Potenza F, et al. The RNA-binding protein PUM2 impairs mitochondrial dynamics and mitophagy during aging. *Mol Cell* 2019;73:775-787.e10. DOI PubMed PMC
82. Galizzi G, Palumbo L, Amato A, et al. Altered insulin pathway compromises mitochondrial function and quality control both in in vitro and in vivo model systems. *Mitochondrion* 2021;60:178-88. DOI PubMed
83. Egan DF, Shackelford DB, Mihaylova MM, et al. Phosphorylation of ULK1 (hATG1) by AMP-activated protein kinase connects energy sensing to mitophagy. *Science* 2011;331:456-61. DOI PubMed PMC
84. Wang XD, Yu WL, Sun Y. Activation of AMPK restored impaired autophagy and inhibited inflammation reaction by up-regulating SIRT1 in acute pancreatitis. *Life Sci* 2021;277:119435. DOI PubMed

85. Choi J, Chandrasekaran K, Demarest TG, et al. Brain diabetic neurodegeneration segregates with low intrinsic aerobic capacity. *Ann Clin Transl Neurol* 2014;1:589-604. DOI PubMed PMC
86. Wan W, Hua F, Fang P, et al. Regulation of mitophagy by sirtuin family proteins: a vital role in aging and age-related diseases. *Front Aging Neurosci* 2022;14:845330. DOI PubMed PMC
87. Karvinen S, Silvennoinen M, Vainio P, et al. Effects of intrinsic aerobic capacity, aging and voluntary running on skeletal muscle sirtuins and heat shock proteins. *Exp Gerontol* 2016;79:46-54. DOI PubMed
88. Kauppila TES, Kauppila JHK, Larsson NG. mammalian mitochondria and aging: an update. *Cell Metab* 2017;25:57-71. DOI PubMed
89. Goldberg EL, Dixit VD. Drivers of age-related inflammation and strategies for healthspan extension. *Immunol Rev* 2015;265:63-74. DOI PubMed PMC
90. Cruz CS, Kang MJ. Mitochondrial dysfunction and damage associated molecular patterns (DAMPs) in chronic inflammatory diseases. *Mitochondrion* 2018;41:37-44. DOI PubMed PMC
91. Gurung P, Lukens JR, Kanneganti TD. Mitochondria: diversity in the regulation of the NLRP3 inflammasome. *Trends Mol Med* 2015;21:193-201. DOI PubMed PMC
92. Licandro G, Ling Khor H, Beretta O, et al. The NLRP3 inflammasome affects DNA damage responses after oxidative and genotoxic stress in dendritic cells. *Eur J Immunol* 2013;43:2126-37. DOI PubMed
93. Crane DD, Bauler TJ, Wehrly TD, Bosio CM. Mitochondrial ROS potentiates indirect activation of the AIM2 inflammasome. *Front Microbiol* 2014;5:438. DOI PubMed PMC